Università degli Studi di Padova

DIPARTIMENTO DI FISICA ED ASTRONOMIA "GALILEO GALILEI"

CORSO DI LAUREA MAGISTRALE IN FISICA

TOWARD A NOVEL SIMPLIFIED MINIATURIZED MICRODOSIMETER FOR THE CLINICAL ENVIRONMENT

Relatore: Dott. Marco Mazzocco

Correlatore: Dott.ssa Valeria Conte

Laureanda: Anna Bianchi, 1130121

Anno Accademico 2016/2017

To my beautiful family
For their love and support

University of Padua

Department of Physics and Astronomy "Galileo Galilei"

Master Degree in Physics

TOWARD A NOVEL SIMPLIFED MICRODOSIMETER FOR THE CLINICAL ENVIRONMENT

Abstract

Radiation therapy with protons and ions is gaining popularity all over the world, because of the physical and biological advances with respect to photon, electron and neutron radiotherapy. At present, sixty-four therapeutic centers worldwide use particle beams to treat their patients. Most of them use fast protons beams and ten centers (3 in Europe, 5 in Japan and 2 in China) use carbon ions.

A definite model of radiation action on living cells is still unestablished, however it is known that the "quantity" of radiation, characterized by the *absorbed dose* (the mean energy imparted to matter per unit mass) is not sufficient to characterize the biological effect, in that equal doses of different radiations lead to different results. Sparsely ionizing radiations, like gamma rays, are less effective than densely ionizing radiations, like slow protons and carbon ions; the capability of ionizing radiation to damage a living cell is closely related to the local energy deposition within relevant subcellular structures indeed, like the chromosomes. An accurate treatment planning should therefore take into account the particle interactions at the micrometer level. To this respect, microdosimetry offers a valuable technique, by measuring the stochastics of energy deposition in small volumes of approximately 1 μm size. Tissue-equivalent gas proportional counters (TEPC) are the reference devices.

A miniaturized TEPC has been built at the Legnaro National Laboratories of LNL, to cope with high intensity therapeutic beams used at the Centro Nazionale di Adroterapia Oncologica (CNAO) of Pavia. The objective of this thesis is to study in detail the working characteristics of this mini-TEPC, with the aim to design a novel simplified microdosimeter optimized for the clinical environment.

Università degli Studi di Padova
Dipartimento di Fisica e Astronomia "Galileo Galilei"
Laurea Magistrale in Fisica

VERSO UN NUOVO MICRODOSIMETRO SEMPLIFICATO E MINIATURIZZATO PER L'AMBIENTE CLINICO

Sommario

La radioterapia con protoni e ioni carbonio sta globalmente guadagnando interesse grazie alla favorevole distribuzione della dose in funzione della profondità (picco di Bragg) rispetto alla terapia con fotoni, elettroni e neutroni. Al momento sessantaquattro centri usano particelle per curare i loro pazienti, la maggior parte usa protoni ed alcuni ioni carbonio.

Nonostante non sia ancora stato definito un modello dell'azione delle radiazioni sulle cellule viventi, è noto che la dose (l'energia media impartita alla materia per unità di massa) non è il solo parametro sufficiente a caratterizzare l'effetto biologico poiché dosi uguali di radiazioni diverse producono effetti differenti. Radiazioni scarsamente ionizzanti, come i raggi gamma, sono meno efficaci di radiazioni densamente ionizzanti come protoni lenti e ioni carbonio; la capacità di una radiazione ionizzante di indurre danni in una cellula è strettamente correlate al deposito di energia locale all'interno delle strutture subcellulari fondamentali, come ad esempio i cromosomi.

Un piano di trattamento accurato dovrebbe quindi tenere conto delle interazioni delle particelle a livello micrometrico. A questo proposito, la microdosimetria offre un valido aiuto, misurando la stocastica del deposito di energia in volumi approssimativamente di 1 μm. A questo scopo i contatori proporzionali a gas tessuto equivalente (TEPC) sono i rivelatori di riferimento.

Un TEPC miniaturizzato è stato costruito ai Laboratori Nazionali di Legnaro dell'INFN al fine di poter misurare anche in campi terapeutici molto intensi come quelli usati al Centro Nazionale di Adroterapia Oncologica (CNAO) di Pavia. L'obiettivo di questa tesi è di studiare in dettaglio le caratteristiche di funzionamento di questo mini-TEPC con lo scopo di progettare un nuovo microdosimetro semplificato ed ottimizzato per l'ambiante clinico.

Aim and outline of the thesis

A miniaturized Tissue Equivalent Proportional Counter (TEPC) has been built at the Legnaro National Laboratories (LNL) of INFN. The counter has a cylindrical cavity of 0.9 mm of diameter and height and 0.81 mm^2 of cross area when the detector is placed with the axis perpendicular to the ion beam. With respect to the commercial FWT LET-1/2 TEPC, the cross area is about 150 times smaller in order to reduce the event rate to sustainable values. Measurements with a prototype mini-TEPC have been already successfully performed with therapeutic proton beams at the Centre Antoine Lacassagne of Nice. The first measurements performed with therapeutic carbon ions at CNAO showed some distortions in the response of the detector, depending on the applied voltage.

The objective of this thesis is twofold. On one hand it aims to study in detail the response function of the mini-TEPC when exposed to high LET radiations, in order to design technical solutions that correct the observed loss of linearity.

On the other hand, it aims to design a novel simplified microdosimeter to be used routinely in the clinical environment. As a relevant simplification in the experimental setup and TEPC operation, the possibility to operate the detector in a gas-sealed mode will be investigated (presently it works in gas-flow mode).

- This thesis is mainly divided into two sections.
    1. The first one comprehends chapters 1 and 2 and it is an introduction to the context and the state of the art.
    2. In the second part, starting from chapter 3, the experimental set up, the methods employed and the results achieved are presented. Finally, a conclusion with a summary of the results and what is left to do ends the work.

An expert reader of this field can skip the introductive part and focus on the experimental section that starts from chapter 3.

<u>INDEX</u>

Chapter 1

Hadron therapy

The second cause of disease in industrialized countries is cancer. As claimed by Agency for Research on Cancer (IARC) [IARC, 2014] in 2012 approximately to 14 million patients were diagnosed with cancer, with the expectation that by 2030 this number will grow up to 21.7 million. Malignant tumours are usually treated with surgery, radiotherapy and chemotherapy or with a combination of them. The choice of cancer treatment depends on the type of tumour, the local size and the presence of metastasis. Radiotherapy with high-energy photons or electron beams represents at present approximately the 50% of treatments of malignant tumours at least in the initial part of their treatment [Durante and Loeffler, 2010].

Hadron therapy is a radiation therapy technique that uses charged particles, such as protons and carbon ions, for treating malignant tumours. Its use is increasing worldwide for treating solid localized tumours because of physical and biological advantages, which result in a better sparing of healthy tissues close to the irradiated target with respect to photon or electron beams. The ideal radiation with which to treat cancer is one that causes death of tumoural cells while sparing the surrounding normal tissue. This is never completely possible, then the goal will be maximum cell killing in the tumour without inacceptable toxicities in normal tissues. In this respect, protons and light ions offer better opportunities as compared to photons and electrons (Figure 1).
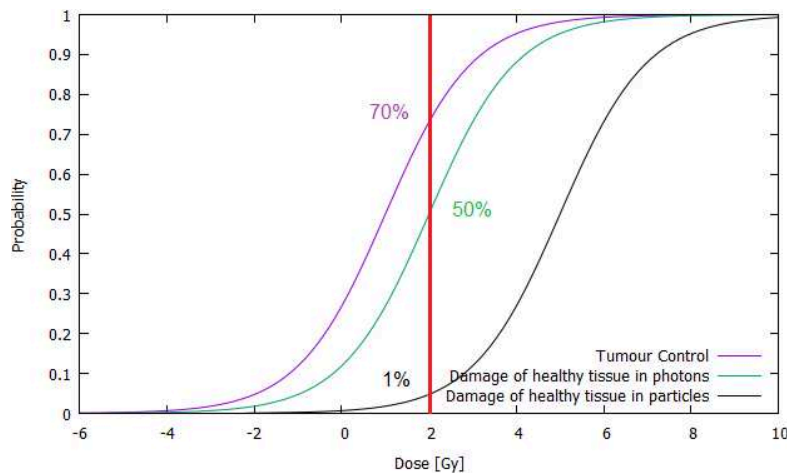
FIGURE 1 - TUMOUR CONTROL (PURPLE LINE) AND HEALTHY TISSUE COMPLICATIONS IN PHOTONS (GREEN LINE) AND CHARGED PARTICLES (BLACK LINE)

The use of charged particles to treat tumours was proposed by Robert Wilson for the first time in 1946. At the beginning most of the hadron therapy centres were based on nuclear physics accelerator like the Lawrence Berkley Laboratories (LBL) in USA. The first patient who was treated in LBL with protons dates back to 1954. The first dedicated hospital-based hadron therapy centre was at the Loma Linda University Medical Centre and started in 1986. From that moment on the number of centres around the world increased allowing the treatment of a large number of patients. According to PTCOG statistics of 2015 around 130 thousand people around the world have been treated with protons and 20 thousand with carbon ions with a total of 150 thousands of people treated with hadron therapy between 1954 and 2015. Currently there are 65 proton and 11 carbon ions centres all over the world.

1.1 <u>Physical aspects</u>

Radiotherapy is related to the use of ionizing radiation to treat malignant tumours. When ionising radiation penetrates into biological tissue, it interacts either directly or indirectly with the DNA, producing lesions of different complexity which finally are translated into a detectable biological effect.

Clearly, the greater the amount of energy deposited by incoming radiation within the target tissue, the greater the induced biological effect. Consistently, the standard quantity used in clinical radiotherapy is the absorbed dose *D*, which according to ICRU Report 85a, is defined by:

$$D = \frac{d\bar{\varepsilon}}{dm}$$
<div align="right">1</div>

Where $\mathrm{d}\bar{\varepsilon}$ is the average energy imparted to matter, $\mathrm{d}m$ is a small element of mass. The unit of absorbed dose is joule per kilogram (J/kg), the special name for this unit is gray (Gy). The absorbed dose is usually measured by means of ionization chambers, calibrated according to dosimetric protocols.

It is worth observing that the energy imparted ε is a stochastic quantity, whereas the absorbed dose *D* is a non-stochastic quantity, as it is illustrated by the following figure.
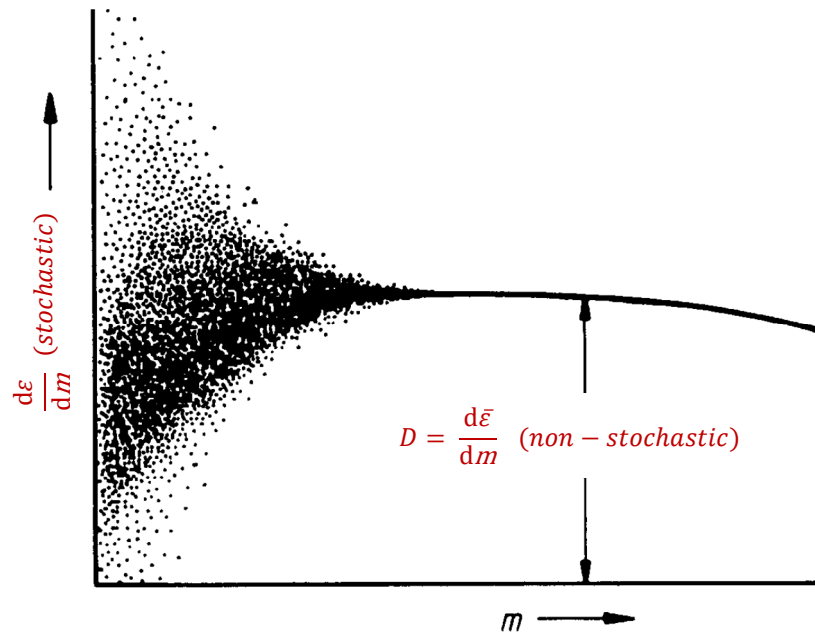
FIGURE 2 - ILLUSTRATION OF THE INCREASING IMPORTANCE OF THE STOCHASTIC OF ENERGY DEPOSITION WITH DECREASING SITE SIZE

The aim of any radiation treatment is to deliver an absorbed dose that is highly conformed to the tumour volume, avoiding irradiating the surrounding healthy tissues as much as possible. With this respect, light ions offer an advantage with respect to photons and electrons, as it is shown in Figure 3.

The absorbed dose profile of photons in matter as a function of depth is a linear-exponential behaviour where the beam releases the most of its energy near the surface decreasing with depth, delivering energy even beyond the tumour. Similarly, with electrons, it is difficult to confine the dose to the desired target volume and a significant part of the total dose is delivered in front of the tumour and beyond it. If protons or carbon ions are used, a lower absorbed dose is deposited near the surface and a steep increase and a sharp fall-off is observed at the end of the range, producing the so-called Bragg peak. This profile in the depth-dose curves is optimal for treating tumours, because it allows sparing healthy tissues around and beyond the tumour.
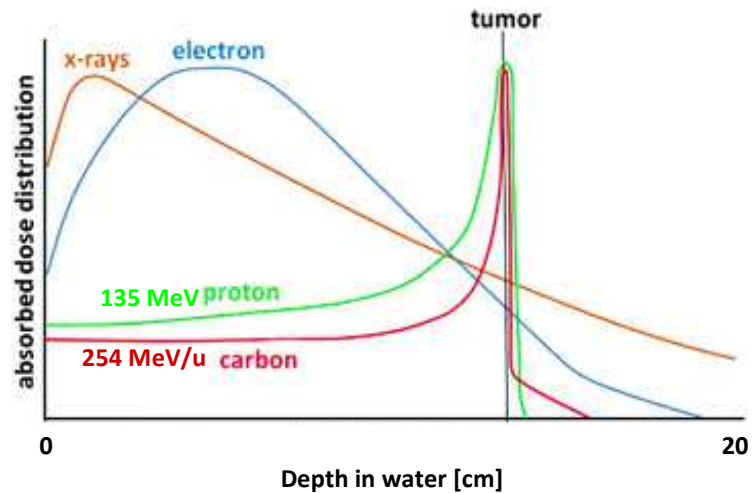
FIGURE 3 - PHYSICAL DOSE AS A FUNCTION OF DEPTH FOR PHOTONS (ORANGE), MONO-ENERGETIC C IONS (RED) AND PROTONS (GREEN) AND ELECTRONS (BLUE)

Some innovative radiotherapy techniques have been developed in the last fifty years to enhance the dose conformity to the tumour volume allowing the treatment of deep tumours even with photons. The low-energy X-rays tubes or radioactive isotopes have been replaced by photons produced in linear accelerators that accelerate electrons from 4 to 25 MeV using microwaves radiofrequency fields. In this way photon beams are indirectly produced accelerating electrons that strike a high-density target that exploiting the Bremsstrahlung effect allow to increase the energy of photons to treat deeper tumours.

With the aim of obtaining a homogeneous absorbed dose, fields coming from several directions are employed to conform the absorbed dose to the tumour sparing normal tissue. To better conform the beam to the shape of the tumour some multi-leaf collimators can be used. Sophisticated and innovative techniques like Intensity Modulated Radiation Therapy (IMRT) provide good conformity of the dose with millimetric precision. Despite of these improvements in the conventional radiotherapy with photons, hadron therapy still are the elective treatment modality in particularly resistant tumour, especially those located close to critical organs.
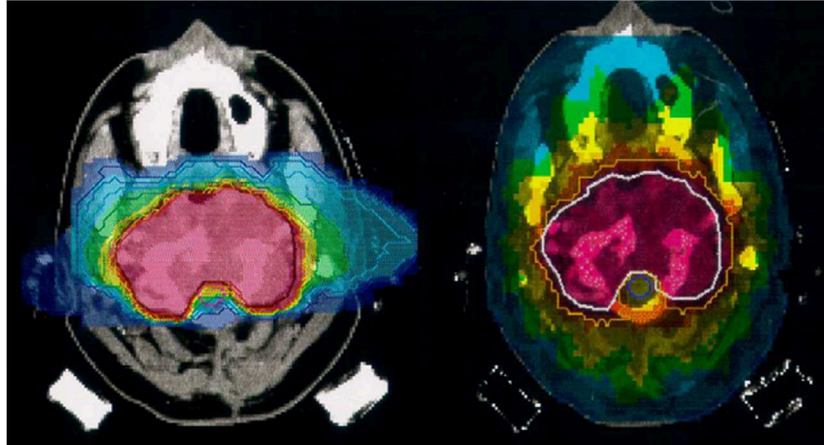
FIGURE 4 - COMPARISON OF THE DOSE DISTRIBUTION IN TRAVERSE PLAN FOR A SKULL BASE TUMOUR USING PROTONS (RIGHT) AND PHOTONS WITH IMRT (LEFT)

The Bragg peak is due to the different modality with which charged particles other than electrons interact with matter.

Charged particles lose their energy following the Bethe equation for the electronic stopping power [G. F. Knoll, 2000, Chapter 2(I)]:

$$S = -\frac{dE}{dx} = const \times \rho \, \frac{Z}{A}\frac{z^2}{\beta^2} \left[ln \left(\frac{2m_e c^2 \beta^2}{I(1-\beta^2)} \right) - \beta^2 \right] \qquad \textbf{2}$$

Where, Z, A, ρ and I are the atomic charge, mass, density and mean ionization potential of the target material. The z and β quantities are the charge and relative velocity (relative to the speed of light) of the projectile. This formula describes the average linear rate of energy loss of a charged particle in a medium.

Besides the superior physical selectivity, the increase of the mass of ions in comparison to light particles (i.e. electrons) reduces the multiple coulomb scattering thus reducing the lateral scattering and the range uncertainties.

On the other hand, charged particles penetrating a medium do not only lose energy through inelastic interactions with the target electrons but also undergo nuclear collisions with the target nucleus, causing projectile and target fragmentation that gives rise to a distribution of secondary light nuclei [Gunzert-Marx et al., 2008] which grows with increasing penetration depth.

5

In case of carbon-ions the projectile fragments play the major role; they have approximately the same velocity of the primary particle and much longer range, as expressed by the following equation:

$$R_{frag} = R_{proj} \times \frac{Z_{proj}^2}{M_{proj}} \times \frac{M_{frag}}{Z_{frag}^2}$$

3

The projectile fragments are responsible for the tail beyond the Bragg peak of carbon ions, visible in Figure 3.

As it is clear from Figure 3, the Bragg peak of mono-energetic particles is too narrow to cover the whole tumour. Usually it is widened by superimposing beams of different energies and intensities to conform the peak to the tumour. The widened peak is commonly referred to as Spread Out Bragg Peak (SOBP).

The SOBP can be obtained with two different techniques: passive delivery in which the beam has a fixed energy and it is then attenuated inserting absorbers of different thicknesses; active delivery where the energy of the beam is modulated from the accelerator.

1.1.1 Passively scattered beam delivery

This technique uses a double scattering system or wobbling-magnets to broaden the particle field. The particle field is then confined into multi-leaf collimators to the tumour cross section. To create the SOBP a rotating modulator wheel is inserted into the beam to periodically change the range. Alternatively to the wheel a static filter of different thickness, the ridge-filter, may be used. The main problems of this method are connected to the high production of secondary neutrons due to the scattering with both collimator and modulator and the high dose released to the healthy tissue because of the inaccurate conformation of the dose to the tumour.
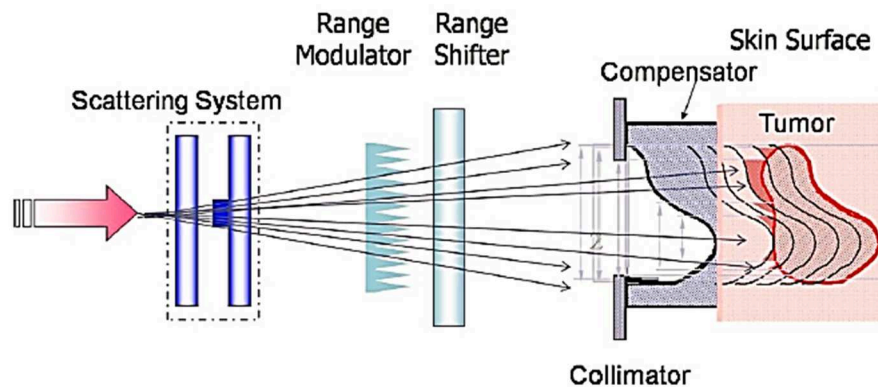

FIGURE 5 - PRINCIPLE OF PASSIVE DOSE DELIVERY [O. JACKEL, 2010]

1.1.2   Active scanning beam delivery

This technique produces a tightly focused pencil beam that is laterally deflected by two magnets allowing scanning the tumour cross section during the treatment. The SOBP is then created changing directly the energy of the beam; this is possible thanks to the use of a synchrotron. In this way, the high dose region is precisely conformed to the proximal end of the target volume and the dose to healthy tissue is minimized.

In the active modality the whole tumour volume is irradiated by painting it voxel by voxel. This technique uses a much higher fluence rate with respect to the passive modality, because the pencil beam impinges on the voxel volume only for a small fraction of the total irradiation time.
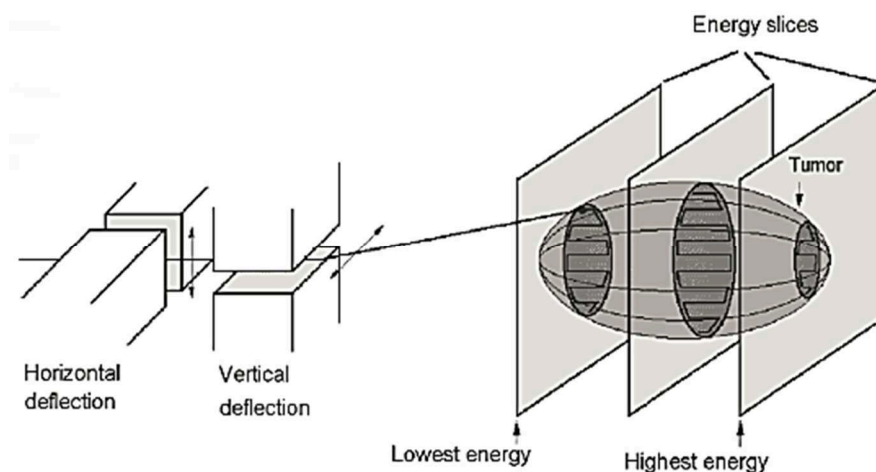

FIGURE 6 - PRINCIPLE OF ACTIVE BEAM SHAPING TECHNIQUE [O. JACKEL, 2010]

1.2 <u>Biological aspects</u>

Cells retain a certain ability to repair DNA, depending on the severity of the initial damage caused by radiations. The initial DNA damage combined with the DNA-repair capability determine the fate of the cells.

In addition to the advantageous conformal physical dose, ions are more effective at killing cells because they create denser ionization events along the particle track, which causes more irreparable damage to DNA than photons.

It is well known that equal doses of different radiations produce different biological effects. The differences in biological effectiveness of a kind of radiation with respect to a reference radiation, usually photons, are described by the relative biological effectiveness (RBE). The RBE is the ratio of the absorbed dose of reference radiation (usually 250 keV X-rays) to the absorbed dose of the specific radiation, which produce the same biological effect (typically a 10% survival level is considered):
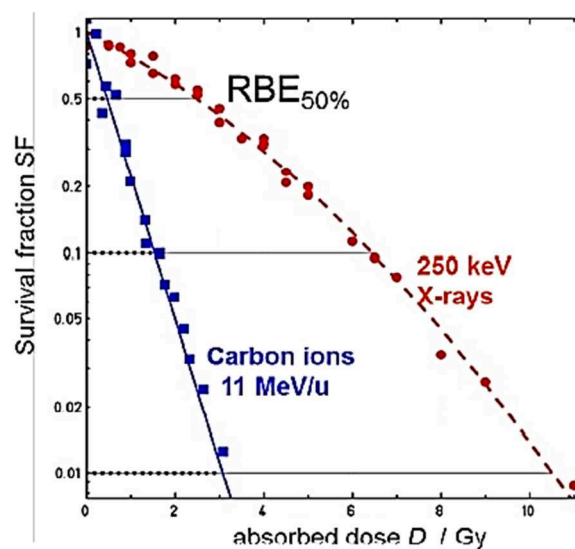
$$RBE = \frac{D_{photons}}{D_{ions}} \qquad\qquad 4$$

D_{photon} and D_{ion} are the absorbed doses for photons and high-LET radiation, which lead to the same biological effect for a given biological system.

Despite its simple definition, RBE is a quite complex parameter because it depends on several physical and biological factors: absorbed dose level, absorbed dose rate, type and velocity of the particle, radiosensitivity of the tissue or cell line, biological endpoint and irradiation modality.

The RBE is derived from cell survival curves, like those shown in Figure 7. In the y-axis the fraction of cells surviving irradiation is plotted as a function of the absorbed dose. In the example the same survival fraction of 10% is achieved with approximately 6.5 Gy of 250 keV X-rays and 1.8 Gy of 11 MeV/u carbon ions. This gives an RBE10 of about 3.6 for the carbon ions.

The Linear Energy Transfer (LET) is the quantity generally used in dosimetry to take into account for the different biological effectiveness of ionizing radiations. The LET is similar to the stopping power except that it does not include the effects of radiative energy loss (i.e., Bremsstrahlung) or delta-rays. Hence, nuclear stopping power is not contained in LET.

The LET is related to the Biological Damage. The severity and permanence of biological changes are directly related to the local rate of energy deposition along the particle track. The higher the LET, the higher the effectiveness of radiation to induce a biological damage. A high LET correlates with a high RBE, as more ionisation events within short distances result in a higher probability of causing clustered DNA damage, which are difficult for the cell to repair. Figure 8 shows a synopsis of RBE values for different cell lines plotted as a function of LET.
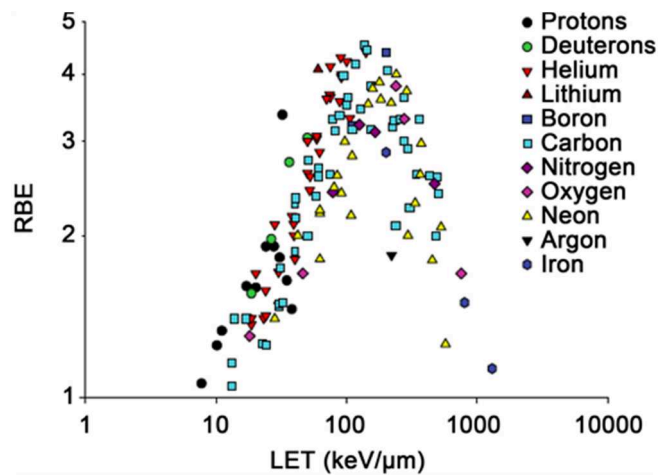

FIGURE 8 - RELATIONSHIP BETWEEN RBE AND LET FOR A MULTITUDE OF HEAVY CHARGED IONS FROM PROTONS TO IRON [S. TEGAMI, 2017]

If we want to understand the dependency of RBE on LET we need to focus on the differences between low LET and high LET radiations. Low LET radiations like X-rays produce a homogeneous dose distribution in the target tumour volume, causing diffuse DNA damage. On the contrary, high LET radiations deposit a large amount of energy in a small distance, resulting in a highly inhomogeneous dose deposition and consequent localized DNA damage.

The decrease of RBE at very high LET values is called overkill effect and starts at LET values around 100-200 keV/μm.

The second biological advantage of ions in comparison to photon radiation, is that low-LET radiation in presence of oxygen causes more biological damage than in hypoxic cells. The ratio of the absorbed doses leading to the same effect in presence and absence of oxygen is called Oxygen Enhancement Ratio (OER). In contrast, high-LET radiation has a lower biological sensitivity to oxygen, leading to a reduction of the OER ratio. Therefore, hypoxic tumours will be significantly less resistant to radiation in case of charged particle beams as compared to photon beams [Tinganelli et al., 2013].

In order to take into account that the same dose of different radiation types produce different effects, the absorbed dose is multiplied by the corresponding RBE value, giving the biological equivalent dose.

Despite the fact that the RBE is a complex parameter, for proton therapy a constant RBE of 1.1 is typically used. However, some theoretical studies [Paganetti, 2003] and experimental measurements [De Nardo et al., 2004b] have shown that deviations from this factor increases dramatically at the distal part of the proton path, demonstrating that the use of a fixed RBE for treatments with protons should be reconsidered. If these differences are not accounted for, such deviations could in some cases result in suboptimal proton treatment plans.

In the case of heavier charged particles, the RBE increases towards the distal edge of the SOBP due to the increase of the LET of the particle toward the end of its range. To compensate this effect, i.e. to obtain a uniform biological response over the tumour, the physical absorbed dose is modulated to produce a lower absorbed dose towards the end of the SOBP. A detailed knowledge of the RBE and its variations inside the irradiated tissue would certainly improve the final success of hadron therapy.

Two approaches can in principle be followed to assess the RBE: a modelling approach [N. Matsufuji, 2007], [M. Scholz et al., 1994] and an experimental approach based on microdosimetry.

In order to optimize the therapeutic plan, the RBE and OER values should be known inside the treatment volume with millimetric spatial resolution. An experimental approach to better know the physical features of the therapeutic beam inside an anthropomorphic phantom could improve the reliability of calculation-based radiobiological parameters. With this respect, microdosimetry offers a valuable aid,

by measuring the stochastic nature of the energy deposition processes in microscopic volumes, with sub-millimetric spatial resolution.

Tissue-equivalent proportional counters (TEPCs) measure the lineal energy spectra in micrometre equivalent sites of complex radiation fields with high precision, since they are able to measure energy deposition events due to less than 3 ionisations (y < 0.1 keV/μm). The full microdosimetric spectrum gives a complete physical description of the radiation-target interaction at micrometre level. It has been demonstrated that microdosimetric spectra can be processed to mimic the radiobiological RBE with good accuracy, if the radio-sensitivity of the irradiated biological system is known for different radiations. The procedure consists on integration of the microdosimetric spectrum after multiplication by a proper empirical weighting function [T. Loncoln et al.,1994], extracted by comparison with radiobiological data. The procedure has been successfully applied to assess with good accuracy the RBE value of neutron and proton therapeutic beams at the Centre Antoine Lacassagne of Nice [L. De Nardo et al, 2004a] [L. De Nardo et al, 2004b]. Basic aspect of microdosimetry and specific aspects related to its application to hadron therapy are developed in the next chapter.

Chapter 2

Microdosimetry

Microdosimetry deals with the description of how the energy is deposited at the subcellular level and the relation with the biological effect produced by different kind of radiations.

2.1 Quantities of Microdosimetry

[ICRU 36, 1983]

The interaction between particles and matter is a discrete process that takes place at specific *transfer points.*

The main quantity is the energy deposit ε_i that corresponds to the energy absorbed at a transfer point:

$$\varepsilon_i = T_{in} - T_{out} + Q_{\Delta m} \qquad\qquad 5$$

where T_{in} is the kinetic energy of the ionizing particle, T_{out} is the sum of all the kinetic energies of the particles leaving the transfer point and $Q_{\Delta m}$ is the change of rest mass energy of the nucleus and particles involved in the interaction.

The total energy imparted to the volume is given by the sum of all the energies imparted to the different transfer points. The number of transfer points is related to the probability of happening of a biological effect.

The most important quantities in microdosimetry are the *specific energy (z)* and the *lineal energy (y).*

The specific energy is defined as:

$$z = \frac{\varepsilon}{m} \qquad\qquad 6$$

Where ε is the total deposited energy and m is the site mass. It is measured in Gray (Gy); it is the stochastic equivalent of the dose that is the limit of z as the mass of the volume tends toward zero.

The lineal energy y is:

$$y = \frac{\varepsilon_1}{\bar{l}}$$ 7

where ε_1 is the energy imparted by a single event, the one caused by a single particle and its secondaries only, and $\bar{l}$ is the average chord length of the volume. Lineal energy is measured in keV/µm and it is the stochastic equivalent of LET. According to the Cauchy's theorem, the mean chord in a convex volume under a uniform and isotropic field of straight infinite lines is:

$$\bar{l} = \frac{4V}{A}$$ 8

Where A is the surface area of the volume V. For a spherical and a right cylindrical cavity:

$$\bar{l} = \frac{2d}{3}$$ 9

Where d is the diameter of the sensitive volume.

For a single event the relation between the lineal energy y and the specific energy z is, in a spherical volume:

$$z = \frac{\varepsilon_1}{m} = \frac{4y}{\pi \rho d^2}$$ 10

They differ for a numerical factor that depends on the geometry of the site size and the density of the target.

Thanks to this formula, a connection between microdosimetric and dosimetric quantities is possible:

$$D = N \frac{\overline{\varepsilon_1}}{m} = N \cdot \overline{y}_F \cdot \frac{4}{\pi \rho d^2}$$ 11

Where N is the number of events that deliver $\overline{\varepsilon_1}$ in the cavity.

2.2 The events distribution

An event in a site is defined as the energy deposited by particles that are statistically correlated and it is the so-called single – event. Since the behaviour of the energy deposit is stochastic, it is necessary to use distributions of probability. The single – event distribution is:

$$f(y) = \frac{dF(y)}{dy} \qquad \qquad \mathbf{12}$$

where F(y) is the distribution of lineal energy under the condition that at least on event happened in the site, and f(y) is the probability of having on event with lineal energy within y an y+dy. The f(y) is normalized to unity and it does not contain the component with y=0, since the particles that cross the site without interactions are not considered by microdosimetry.

The dose distribution of the lineal energy is the fraction of absorbed dose with lineal energy less or equal to y.

The dose probability density is:

$$d(y) = \frac{dD(y)}{dy} \qquad \qquad \mathbf{13}$$

The first moment of the distribution id the frequency – mean lineal energy:

$$\overline{y_F} = \int_0^\infty y f(y) dy \qquad \qquad \mathbf{14}$$

The relation between d(y) and f(y) is:

$$d(y) = \frac{1}{y_F} y f(y) \qquad \qquad \mathbf{15}$$

The second moment is the dose – mean lineal energy:

$$\overline{y_D} = \int_0^\infty y d(y) dy = \frac{1}{y_F} \int_0^\infty y^2 f(y) dy \qquad \qquad \mathbf{16}$$

Similarly, probability distributions f(z) and average quantities $(\bar{z}_F, \bar{z}_D)$ are defined for the specific energy z.

The specific energy z is a stochastic quantity but it can represent the sum of the energy imparted by more than one event.

2.3 <u>Microdosimetric spectral analysis</u>

Microdosimetry analyses several kind of radiation fields and therefore lineal energy can span over four or five orders of magnitude. Because of this, the usual representation of a microdosimetric spectrum is semi – logarithmic, y in logarithmic

scale on the axes of abscissas and yd(y) in linear scale on the axes of ordinates. In this representation, the area under the curve between two y-values is proportional to the fraction of dose delivered by events with lineal energies in this range.
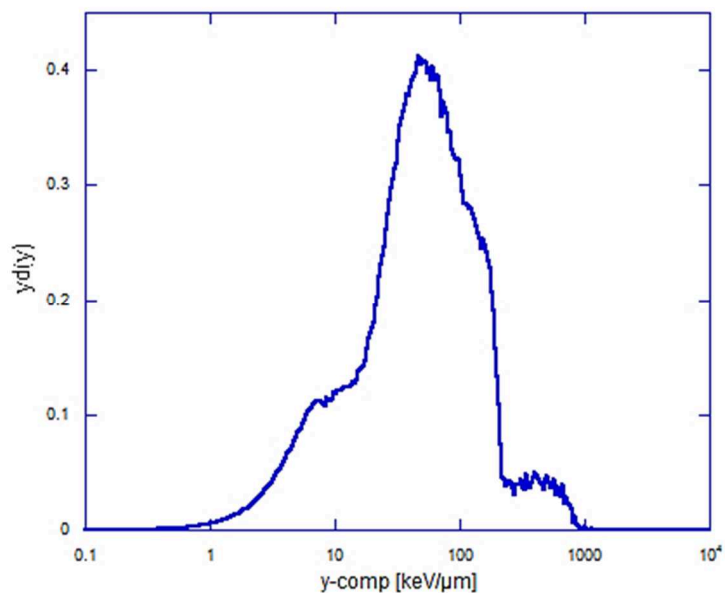

FIGURE 9 - MICRODOSIMETRIC SPECTRA OF A NEUTRON RADIATION FIELD OBTAINED WITH A MINI TEPC IN LNL

This is an example of microdosimetric spectrum in a neutron field.

In the image below the same spectrum has been divided into three color-coded areas.
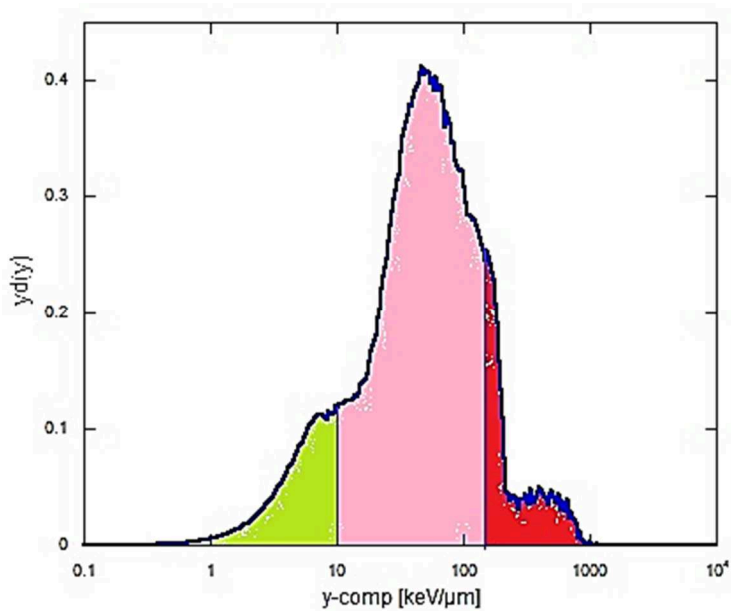

FIGURE 10 - THE SAME SPECTRA OF FIG. 9 DIVIDED INTO AREA OF DIFFERENT LET RADIATION

The green area corresponds to events due to low LET radiation and it represent approximately the 13% of the total dose; the pink part is due to medium LET radiation, e.g. protons, and it is about 75% of the total area; finally the red part is approximately 12% of the entire dose and it is associate with high LET events.

2.4 <u>Microdosimetric Radiation quality</u>

The microdosimetric distribution provides information about the radiation quality of a beam and it helps to estimate the biological effectiveness and to understand how the radiation field changes in depth in the tissue.

The following measurements were performed with a LNL mini-TEPC in Nizza [L. De Nardo, 2004a] and it showed that the microdosimetric spectrum changes and a major contribution of high LET radiation is observed going deeper in the SOBP.
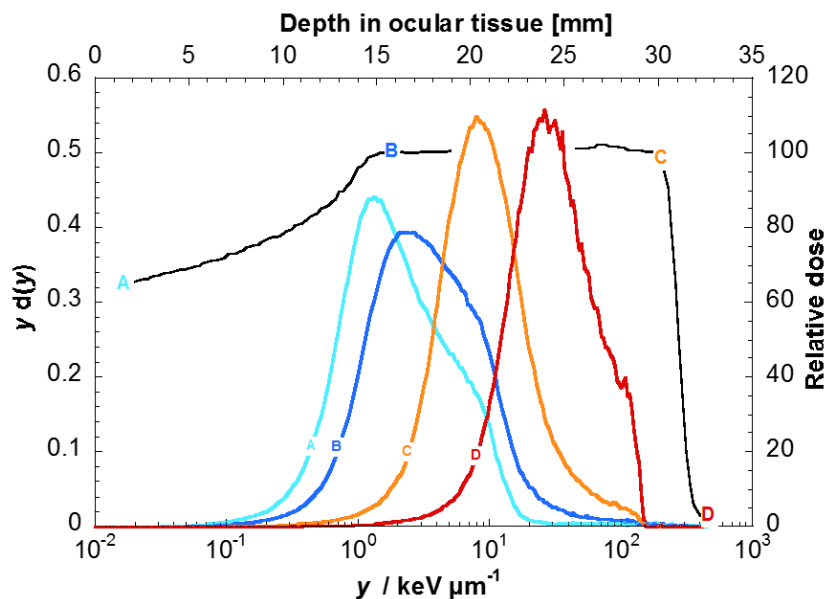

FIGURE 11 - MICRODOSIMETRIC SPECTRA COLLECTED AT FOUR DIFFERENT DEPTH IN THE NICE THERAPEUTIC PROTON BEAM [L. DE NARDO, 2004A]

Microdosimetry is a useful tool to estimate the biological effectiveness of a radiation field using physical data. The microdosimetric spectra can be used to assess the microdosimetric RBE doing a convolution with a weighting function.

$$RBE_\mu = \int_0^\infty r(y)d(y)dy$$ 17

17

The function r(y) is the weighting function obtained in radiobiological experiments in several radiation fields with different cell lines. The aim of this function is to mimic the biological behaviour of irradiated cells. Three different r(y) functions have been proposed in the past derived from both microdosimetric spectra and radiobiological data. Figure 12 shows the r(y) calculated in 1990 by Pihet et al. for 8Gy given in one fraction in a 2µm site size that was derived from radiobiological and microdosimetric measurements in neutron therapy beams [P. Pihet,1990]. The plateau at the beginning of the plot in Figure 12 is associated with low LET radiation (y ≤ 10 keV/µm), and then it increases up to a maximum of 70 keV/µm due to high LET radiation. After this maximum it becomes lower than one, this phenomenon is explained by the overkill effect, higher y-values do not induce an additional biological effect. A similar effect is also observed in RBE vs. LET curves.
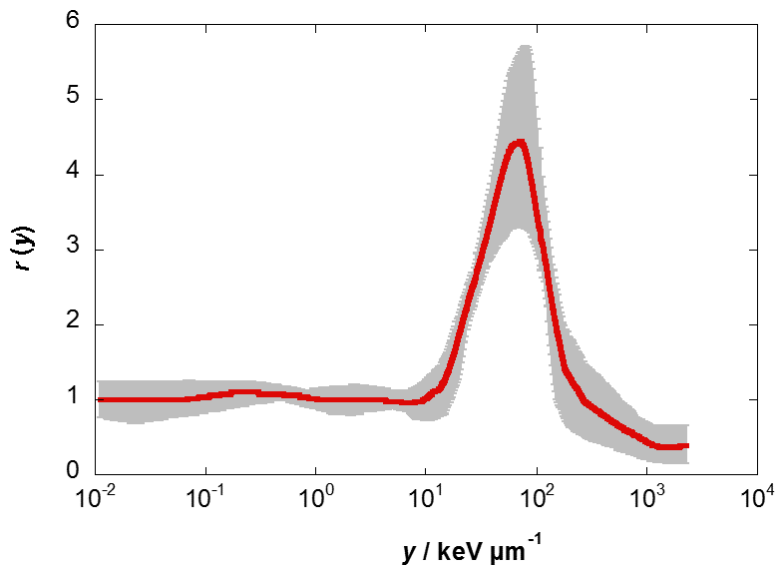

FIGURE 12 - BIOLOGICAL WEIGHTING FUNCTION FOR INTESTINAL CRYPT CELLS REGENERATION IN MICE FOR 8 GY DERIVED FROM NEUTRON THERAPY BEAMS (RED LINE) AND STANDARD DEVIATION (GREY AREA) [P. PIHET, 1990]

The application of the weighting function to microdosimetric spectra allows determining the RBE performing microdosimetric measurements.
Some measurements were performed with LNL mini-TEPC to assess the radiation quality of the Nice therapeutic beam [L. De Nardo, 2004a] with the result that the microdosimetric RBE can mimic the trend of the radiobiological RBE and for this reason it is feasible to improve this technique for online measurements of the quality of the beam (Figure 13).

The overall uncertainty of the REB$_\mu$ depends on the uncertainties of r(y), d(y) distributions, the calibration procedure of y and the TEPC detection efficiency. The weighting function is not a universal function, it depends on the beam, the cell line, the biological endpoint, the simulate site and the absorbed dose. Before starting to use a microdosimeter as an online monitor of radiation quality, radiobiological and microdosimetric studies have to be performed on the beam with the purpose to extract the weighting function.
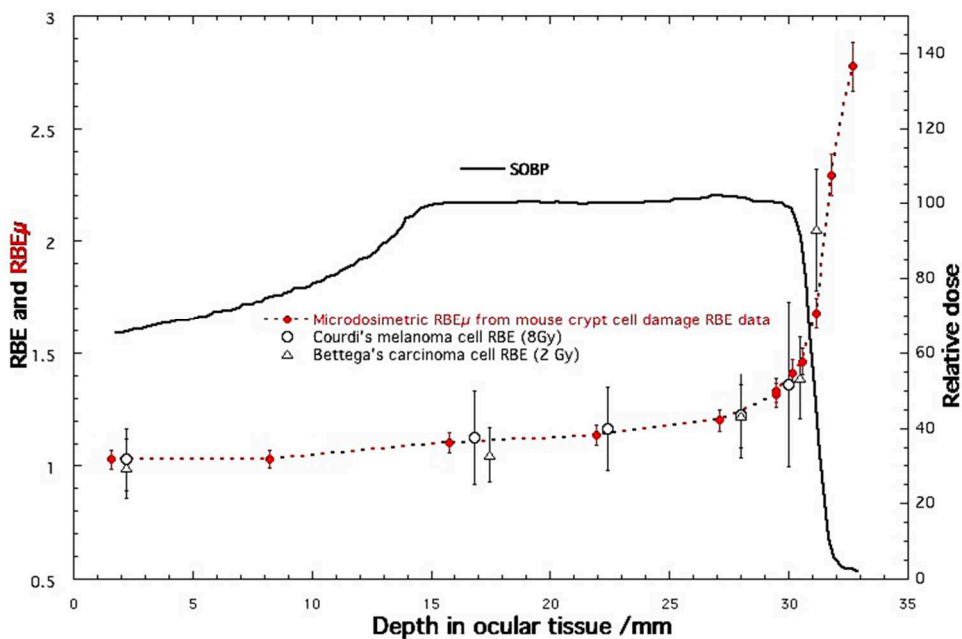

FIGURE 13 - COMPARISON BETWEEN RADIOBIOLOGICAL AND MICRODOSIMETRIC RBE AT THE NIZZA THERAPEUTIC PROTON BEAM [L. DE NARDO, 2004A]

2.5   Detectors employed in microdosimetry: TEPC

Tissue Equivalent gas Proportional Counters are the reference detectors used in microdosimetry. There are also other kinds of detectors employed such as silicon detectors and diamond detectors.

TEPCs measure the distribution of ionizations in the sensitive volume later converted to a distribution of lineal energy through a proper calibration.
Proportional counters are gas-based detectors filled with tissue equivalent gas, usually propane or propane-TE. They work in pulse mode, each ionization event occurring in the chamber gives rise to a signal pulse.

19

TEPC consists into two electrodes, a central anode surrounded by a conductive wall that works as the cathode. When a potential difference is applied to anode and cathode an electric field is generated inside the chamber directed from the anode to the cathode. Thanks to this electric field, the negative charges created by the ionization process drift toward the anode. The electric field divides the sensitive volume into two imaginary areas, the drift zone and the multiplication zone. The electrons created in the ionization events move towards the anode thanks to the drift zone. In the multiplication zone the electric field is higher than in the drift zone and primary electrons gain kinetic energy and if this energy is high enough they can ionize the gas and create secondary electrons.
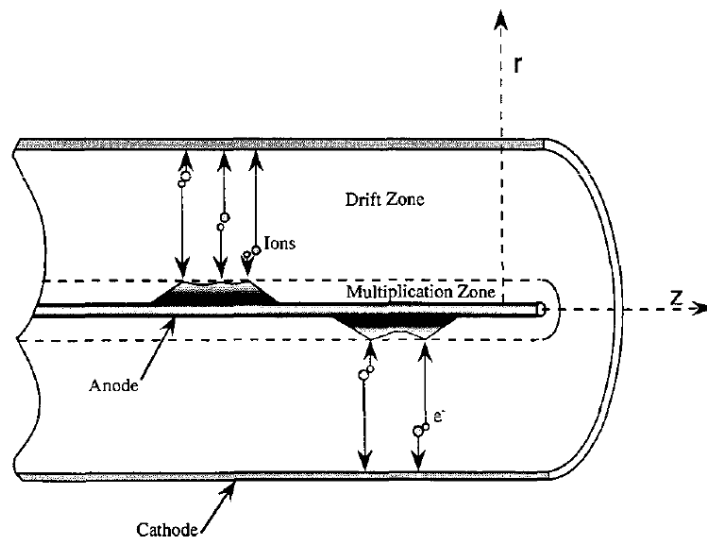
FIGURE 14 - SECTION OF THE TEPC WHERE IS EXPLAINED THE GEOMETRY OF THE ELECTRIC FIELD [D. MORO, 2006]

At the atmospheric pressure, the gas gain mainly takes place within 3-5 anode radii. Real gas amplification starts when the electric field becomes greater than a critical value E_c. This value is a gas characteristic and for most gases is in the range 30-70 kV/cm at the atmospheric pressure or $S_c \approx 40$-90 V/cm·Torr in terms of reduced electric field.

The electric field in a cylindrical counter is:

$$E(r) = \frac{V_a - V_c}{r ln\left(\frac{r_c}{r_a}\right)}$$
18

This process creates an avalanche of ionizations with the final consequence of a larger output pulse. They are called proportional counters because the number of

charges produced in the avalanche is proportional to the number of primary electrons produced in the chamber. The proportionality factor is called gas gain.

2.5.1 Gas Gain

[P. Segur, 1995]

The gas gain depends on various parameters: the geometry of the detector, diameters of anode and cathode, the filling gas, its pressure and the potential difference applied to the electrodes. It is defined as the mean number of electrons collected by the anode per ion pair produced by the primary ion. The gas gain is linked to the Townsend first – ionizing coefficient α_t that gives the number of ion pairs generated by the primary electron per unit length:

$$n(d) = n_0 e^{\alpha d} \qquad \text{19}$$

where d is the distance travelled by the electron and n_0 is the number of primary electrons.

Using the first – ionization coefficient the gas gain is:

$$\ln(G) = \int_{r_c}^{r_a} \alpha_t dr \qquad \text{20}$$

where r_c and r_a are the cathode and anode radii.

The first – ionization coefficient decreases with decreasing electric field and with increasing gas pressure, this is because a smaller electronic mean-free path prevent electrons to reach the energy to cause secondary ionizations.

In a cylindrical sensitive volume the reduced electric field is:

$$S = \frac{E}{N} = \frac{V_a - V_c}{rN \ln\left(\frac{r_c}{r_a}\right)} \qquad \text{21}$$

where N is the gas number density.

The dependence of α/N on the reduced electric field S is quite complicated, thus several models have been developed to describe the gas gain in proportional counters. Two main models are now illustrated.

2.5.1.1 Classical gas gain theory

In this approximation, the Townsend first-ionization coefficient only depends on S and the electrons are in the equilibrium state. Electrons are in equilibrium with the electric field when and only the normalized electron distribution function and the electric field are spatially independent [K. Mitev, 2005]. This model is based on semi-empirical analytical expressions that are easy to use and often they can estimate the gas gain parameters in an acceptable way.

The reduced Townsend coefficient is:

$$\frac{\alpha}{N} = \frac{L}{V_i} S^m e^{\frac{-L}{S^{1-m}}} \qquad\qquad \textbf{22}$$

where V_i is the effective ionization potential and $L = hcV_i$, $h = \lambda/\lambda_{coll}$, λ_{coll} is the projection of the distance between two ionization events. The parameters L, V_i and m are characteristics of the counting gas.

When this expression of the Townsend coefficient is used in the expression of the reduced gas gain the result is:

$$\frac{lnG}{K} = \frac{1}{1-m}\frac{L}{V_i}\left(e^{-LS_a^{m-1}} - e^{-LS_c^{m-1}}\right) \qquad\qquad \textbf{23}$$

This result is obtained assuming that the ionization coefficient, the drift velocity and the diffusion coefficient depend only on the reduced electric field at a given point in the sensitive volume. This is called equilibrium assumption, under this condition the ionization coefficient of a non-homogeneous electric field is the same as that of a homogeneous field of the same strength. The equilibrium value of the reduced ionization coefficient does not depend on gas pressure. This assumption is true at gas pressure high enough that the variation of the electric field over the mean-free electron path is low.

For this reason at low gas pressure the classical gas gain theory cannot be applied, the electric field changes considerably along the mean-free path of the electrons contrasting the basilar condition of the equilibrium assumption. A further development of this model is the gradient field model.

2.5.1.2 Gas gain gradient field model

Segur et al. (1995) developed an analytical model that takes into account the non-equilibrium effects on the gas gain. The electrons are not in equilibrium with the electric field when the normalized electron distribution function depends directly on the position of electrons [K. Mitev, 2005]. Considering the gradient field between two consecutive ionizations, the reduced Townsend coefficient is:

$$\frac{\alpha}{N} = \frac{L}{V_i} S^m e^{MS^{m-1}} \tag{24}$$

Where $M = \frac{L}{V_i} K e^{\frac{V_i}{K-1}}$.

Replacing this expression in the equation of the reduced gas gain the result is:

$$\frac{lnG}{K} = \frac{L}{MV_i(1-m)} \left(e^{-MS_a^{m-1}} - e^{-MS_c^{m-1}} \right) \tag{25}$$

In homogeneous electric fields the plot of the reduced gas gain ln(G)/K at different pressures is a single curve while under conditions of non-equilibrium it does not lie in a single curve but in several curves that depend on different K-values. It is observed from experimental data that at the same S_a the gas gain increases with the applied voltage difference and that a saturation effect occurs as the voltage difference increases.
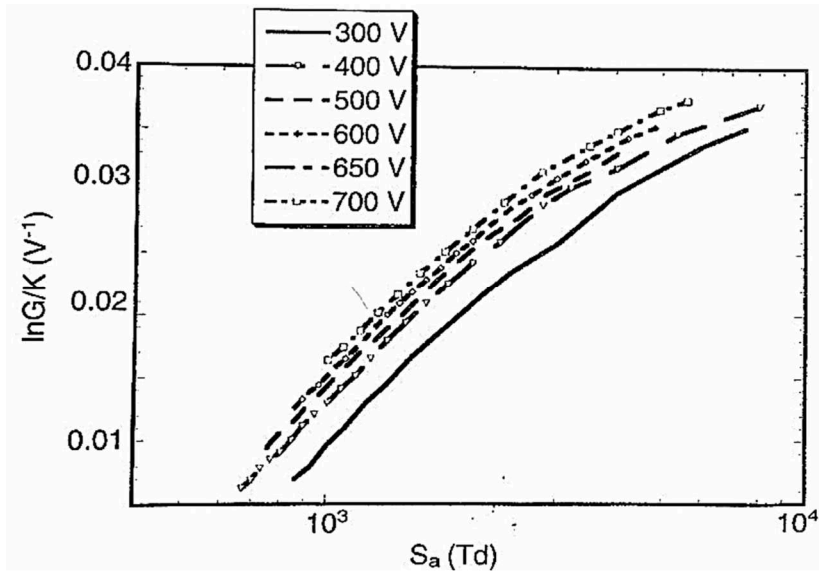

FIGURE 15 - VARIATION OF THE REDUCED GAS GAIN AS A FUNCTION OF THE ELECTRIC FIELD AT THE ANODE IN METHANE-BASED TE GAS MIXTURE [P. SEGUR, 1995]

2.5.2 Conversion from ionization yield and imparted energy

TEPCs measure the number of ionizations produced by charged particles in the gas, afterwards the ionization spectrum is interpreted in terms of energy imparted spectrum by assuming that, on average, the same amount of energy (W) is spent for producing an electron-ion pair.

The particle loses all its energy not only by ionization processes but also with excitations, for this reason the W-values is approximately twice the ionization potential. For a given gas type, a constant W is generally assumed, even if W depends on particle type and energy. The differential $W(E)$ decreases with increasing kinetic energy becoming almost constant at high particle energy while $W(E)$ increases when the particle velocity is comparable to that of orbital atomic electrons of the gas. W-values increase with particle mass and decrease with particle energy. When the variation of the W in the detected radiation field is large, the assumption of proportionality between the ionization spectrum and the imparted energy spectrum should be considered prudently.

2.5.3 Simulation of the site

TEPCs have been developed to simulate the energy deposition in microscopic volumes of biological tissues, for this reason they are made of tissue-like materials and they are filled with tissue equivalent gas. They are made of a mixture of mainly H, C, N and O in percentages similar to those found in human body. The main gas mixture used in microdosimetry are methane-based TE (64.4% CH_4, 32.4% CO_2 and 3.2% N_2) and propane-based TE (55% C_3H_8, 39.6% CO_2 and 5.4% N_2), the last one offers better gas gain properties. However, it has been demonstrated that it is possible to use pure propane instead of propane-based TE gas even if the cross section in pure propane is higher than that of propane-TE resulting in a higher number of events in pure propane, if the mass per area in pure propane is reduced of a factor 0.75. [S. Chiriotti, 2015].

The detector is made of A150 plastic which is a TE conductive plastic (10.1% H, 77.6% C, 3.5% N, 5.2% O, 1.7% F) that is also the detector cathode. The simulation principle is based on the concept of equal energy released to gas cavity and the microscopic volume simulated. The aim of the simulation is to have the same mean

imparted energy in a sphere of tissue with d as diameter and a sphere of gas with D as diameter. The energy imparted is the result of the multiplication of the mass stopping power and the mass path length across the site [ICRU 36, 1983]:

$$\varepsilon_t = \left(\frac{S}{\rho}\right)_t (d\rho)_t = \varepsilon_g = \left(\frac{S}{\rho}\right)_g (D\rho)_g \qquad 26$$

Where $\frac{S}{\rho}$ are the mass stopping power and $d\rho$ are the mass per area in tissue and gas. To be sure that the secondary particle fluence is independent from the density, the atomic composition of the wall and the gas must be identical as stated by the Fano theorem [U. Fano, 1954]. Using this theorem, if gas and tissue have the same atomic composition, the stopping powers can be assumed as equal for the radiation considered. Thus the equation to simulate the given site size is:

$$(d\rho)_t = (D\rho)_g \qquad 27$$

Once obtained the gas density, it is possible to find the pressure inside the cavity linked to the site size using the ideal gas law:

$$P = \frac{\rho_g}{\rho_0} \frac{P_0 T}{T_0} = \frac{d_t \rho_t}{D_g} \frac{1}{\rho_0} \frac{P_0 T}{T_0} \qquad 28$$

Where ρ_0 is the gas density at $T_0 = 273.15$ K and $P_0 = 101325$ Pa.

2.5.4 Particle tracks

It is possible to distinguish into five different classes of particle tracks in the cavity [R. S. Caswell, 1966]. The different type of tracks are connected with some features of microdosimetric spectra, e.g. the edges that are useful for calibration purposes.
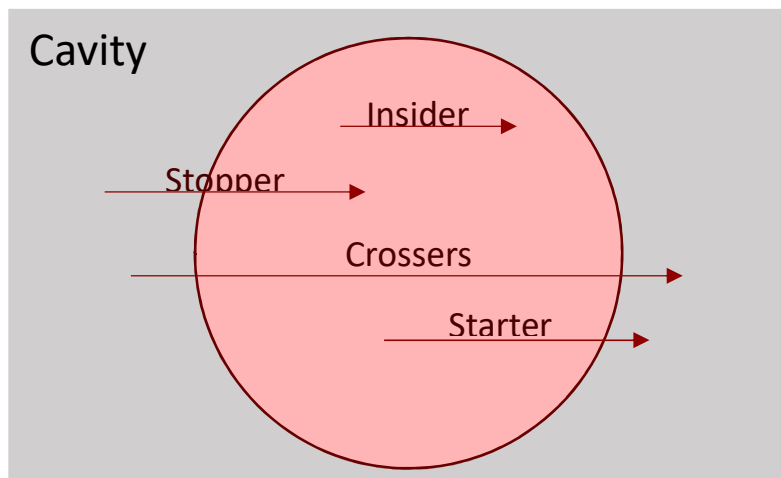

FIGURE 16 - REPRESENTATION OF THE DIFFERENT TRACKS OF THE PARTICLES INSIDE THE SENSITIVE VOLUME

- *Crossers:* particles generated outside the volume with enough energy to cross the whole volume releasing just part of their energy
- *Starters:* particles generated in the volume able to leave the volume depositing just part of their energy
- *Stoppers:* particles generated outside the volume that completely stop inside the volume
- *Insiders:* particles generated inside the volume that stop before going out
- *Touchers:* particle generated outside the volume that do not enter it in a straight line but by struggling, or just their delta rays enter.

A microdosimeter does not give any information on the particle track structure because it integrates the number of ionization inside the sensitive volume. Information on the particle structure can be obtained with nanodosimetric measurements.

2.6 <u>Microdosimetry applied to hadron therapy</u>

The typical maximum event rate sustainable by a proportional counter is about 100 kHz, condition that is easily exceeded in high-intensity clinical-beams as those delivered in active-scanning modality. For instance, the minimum therapeutic carbon ions fluence rate available at CNAO is ~ 10^5 $mm^{-2}s^{-1}$.

Most of microdosimetric measurements of carbon ion beams have been performed in the past with commercial TEPCs, like the Far West Technologies (FWT) LET-½ spherical tissue-equivalent proportional counter, which is a relatively large detector with a cross area of 127 mm^2 (a sphere of 12.7 mm of diameter). These TEPCs have limited capability to measure at high fluence rates. They were used in low-intensity continuous beams or in conjunction with rather cumbersome trigger and veto detection systems to prevent spectral distortions due to pile-up effects.

For a given sustainable event rate, the acceptable fluence rate depends on the cross area of the detector. To cope with high intensity therapeutic ion beams it is necessary to reduce the geometric size of the TEPC. A new mini-TEPC has been developed at the Legnaro National Laboratories (LNL) of the Istituto Nazionale di Fisica Nucleare (INFN) of Italy. The counter has a cylindrical cavity of 0.9 mm of diameter and height and 0.81 mm^2 of cross area when the detector is placed with the

axis perpendicular to the ion beam. Since the cross area of the mini-TEPC is about 150 times smaller than the area of the FWT LET-1/2, it is expected that the sustainable fluence rate is correspondingly 150 times higher.

2.6.1 State of the art and problems

The first measurements in actively scanned beams performed with a similar mini-TEPC, have showed some limits in the detector response that need to be systematically investigated. The LNL mini-TEPC was firstly tested in low LET radiation field with good results that underlined a linear response of the detector. However, the same result was not achieved in high LET radiation field where a severe loss of linearity was observed. High-LET radiation fields generate a high ion density around the anode, which could cause significant distortions of the electric field inside the sensitive volume.

These results were presented in E. Motisi's master thesis (2015). The conclusions of that work were that for low-LET radiation fields the microdosimetric spectra retain the same shape changing linearly in the gas gain with the voltage applied. At that moment was observed that for high-LET events the spectra shape were distorted when high gas gain were employed, while at lower applied voltages the spectra had the same shape. For this reason, in order to work with a large range of events sizes, the best option seemed to acquire the microdosimetric distributions with two different gas gain. The two spectra were then joined offline using the lower part of the spectrum with high gain and the highest part of that with low gain.

This was a preliminary solution that needed to be further investigated and validated.

This thesis is the continuation of that study and has the aim of doing a systematic characterization of the detector under the irradiation of a high-LET radiation field analysing the response of the detector changing different parameters, e.g. the voltage difference applied and how it is divided between anode and cathode.

Already built detectors in LNL work in gas flow mode, some preliminary tests were also performed during this master thesis with the aim of assessing the feasibility of using these devices in gas-sealed mode. Encouraging results were obtained in low LET radiation fields but other tests in high LET radiation are needed. A sealed TEPC would be an optimal simplification for the clinical environment reducing the volume of the experimental set up moved to measure in clinical facilities.

Chapter 3

Experimental Set Up

The following chapter contains a description of the experimental set up: the detector, the electronic chain and the gas system.

3.1 Mini-TEPC

The detector used in this thesis in the LNL mini-TEPC AMICO 7. The cylindrical cavity of this TEPC is 0.9 mm of diameter and height that corresponds to a sensitive volume of 0.6 mm^3. The anode is a golden tungsten wire of 10 µm of diameter. The detector is inserted in a titanium sleeve of 2.7 mm of diameter and 20 cm of length, the external size of this mini-TEPC corresponds to an 8 French[1] catheter and it could be ideally used in *in vivo* microdosimetry. An *in vivo* experimental use of this detector is far from being reality, but its shape makes it easier to use in phantoms simulating the depth in the tissue. Its small dimensions reduce uncertainties in positioning it in order to guarantee a more precise study of the beam in depth in the tissue. It works in gas flow mode usually at a simulated site size of 1 µm.
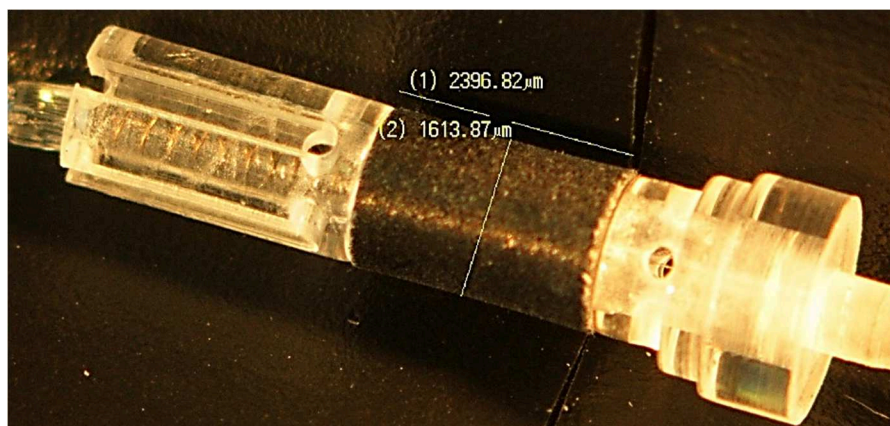
The assembled detector:

FIGURE 17 - AMICO 7 DETECTOR

---

[1] The French scale is the unit commonly used to measure the size of catheters.

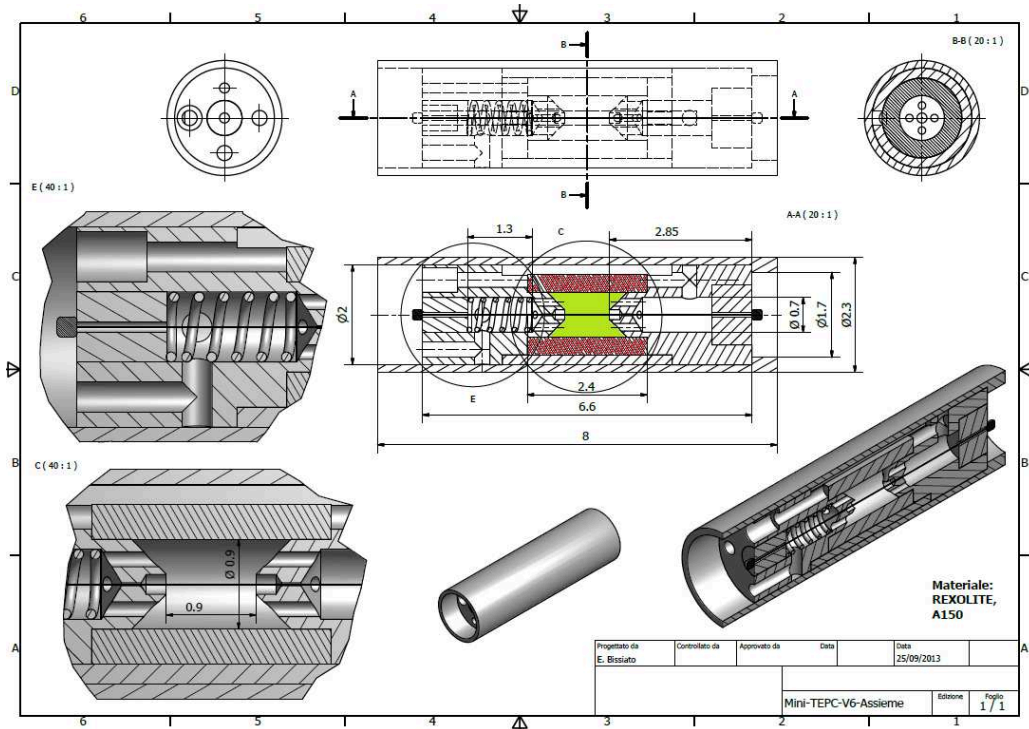In the following picture is represented the project of the detector:

FIGURE 18 - PROJECT OF THE AMICO 7 DETECTOR, IN GREEN THE SENSITIVE VOLUME, IN RED THE CATHODE MADE OF A150 PLASTIC

The following picture shows the detector inside the sleeve, the aluminium box under the sleeve contains the electronic front-end and the yellow and blue connectors are the feedthroughs for the gas and flow system.
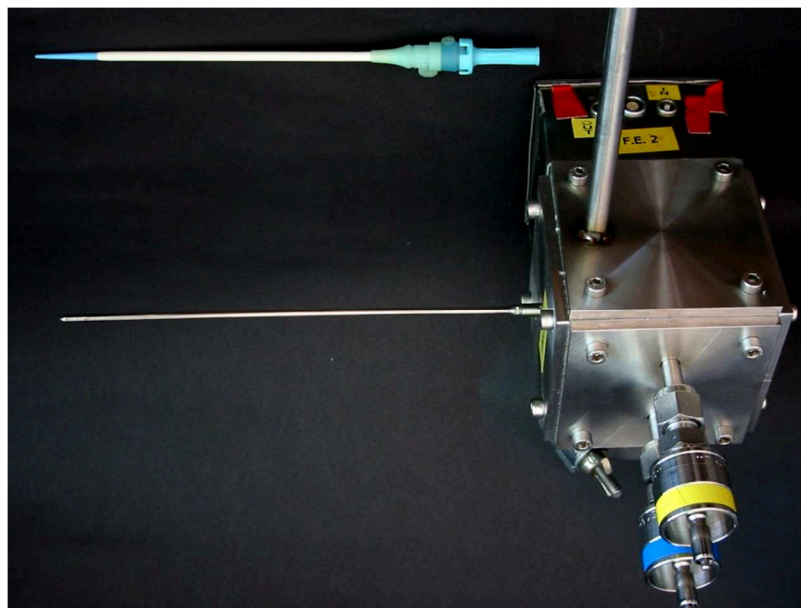

FIGURE 19 - PHOTO OF AMICO 7 INSIDE THE TITANIUM SLEEVE WITH THE CONNECTOR OF THE IN/OUT GAS ANT THE BOX OF THE ELECTRONIC OF FRONT-END

3.2 **Electronic chain**

TEPC operates in pulse mode, recording charged particle tracks as a pulse-height single-event spectrum.

Depending on the radiation field, the pulse height spectrum can extends over a large (5 decades) dynamic range. For this reason, negative pulses collected at the anode are fed into a low noise charge-sensitive preamplifier of 300 electrons RMS noise with a dynamic range of $5 \cdot 10^4$. The preamplifier has to be positioned as close as possible to the TEPC to maximize the signal-to-noise ratio. The preamplifier converts the pulses into exponentially decaying signals whose height is proportional to the energy of the primary ionization. The output signal is a positive pulse with a fast rise time (<10 ns) and a decay constant of 50 μs.

Typically, the microdosimetric spectrum is represented in a semi-logarithmic graph, with the lineal energy on the x-axis in a base 10 logarithmic scale, and 60 points per decade. To ensure a good resolution to the whole spectrum (at least 3.5% as required by the logarithmic binning), the output from the preamplifier is fed into three linear amplifiers that integrate and amplify the signal with different gains, usually with a multiplication factor of x1, x10, x100. The output of the amplifiers is a Gaussian shaped voltage signal with an amplitude up to 10 V.

The analog signals from the three amplifier are then converted by three different ADCs (Ortec Models AD114 and AD413), histogrammed in three histogramming memories, finally the three sub-spectra are processed and joint offline to obtain a complete spectrum.
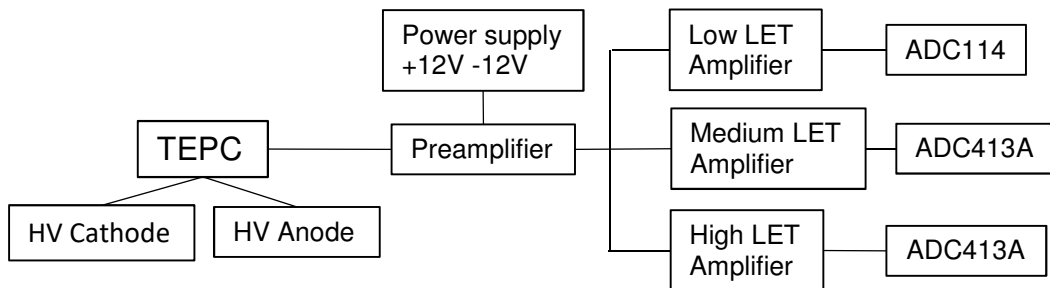

FIGURE 20 - SCHEME OF THE ELECTRONIC CHAIN USED IN MICRODOSIMETRIC MEASUREMENTS

The electronic chain used in this thesis is huge and heavy. One of the things that should be done in the near future to make this detector easier to move and use in a clinical environment is to reduce the size of the electronic chain.

3.3 Gas system

The type of gas used in the detector influences the gas gain and the response function of the detector. The most frequently employed gases are methane, propane and methane or propane-based mixtures. In this study only pure propane has been used as the equivalence of the use of pure propane and propane-TE with a correction factor has been demonstrated [S. Chiriotti et al., 2015] (see § 2.5.3). The gas should be highly pure to guarantee the reproducibility of microdosimetric measurements because impurities can decrease the stability of the gas gain while measuring.

There might be three important sources of contamination in the gas of the detector.

The first one is outgassing, this phenomenon occurs when the inner surface of the detector absorbs gases, e.g. water vapour or oxygen, and they are then re-emitted into the cavity causing a gradual change in the gas mixture. Small contaminations of electronegative gases, as those mentioned above, decrease gas gain because they capture electrons and produce negative ions that slow down fast electrons going towards the anode.

The second cause of contaminations is leakage, which must be prevented while constructing the detector and the flow and vacuum system.

The last cause of contamination is due to the interaction between particles and gas molecules that, breaking the chemical bonds of the gas, creates polymers that can deposit on the surface of the anode wire increasing its effective diameter. Though the absolute number of these polymers is very low as compared to the Avogadro number, the ageing effect due to the formation of insulating layers on the anode wire can be significant. The presence of the insulating deposit modifies the space-time distribution of the electric field near the wire surface where the avalanche formation takes place, generally resulting in a decrease of the gain in long term operation.

To avoid gas contamination and ageing effects, the detector is connected to a gas flow and vacuum station. Before starting to use the mini-TEPC some days of vacuum are needed to prevent outgassing forcing the absorbed substances to come out from the surface. The vacuum is provided by means of a turbo pumping station, HiCube 80 by Pfeiffer Vacuum that maintains a stationary vacuum level of 10^{-6}-10^{-7} mbar. After some days of vacuum in the whole system (detector and vacuum station) where

the only closed valve is that of the gas (V4, sketch below) the detector is ready to be filled with gas.

In order to maintain a stable gas pressure inside the sensitive volume the pressure is controlled both at the entrance and at the exit of the detector. The gas flows into the mini-TEPC and an absolute pressure transducer measures the entrance pressure. At the exit of the detector there is another absolute pressure transducer. This kind of pressure transducer does not depend on the gas composition, it has a precision of 0.1 mbar and an accuracy of 0.12%, as indicated by the manufacturer. The pressure transducer that controls the gas exit is also the controller of an electric solenoid valve that regulates the gas exit. It is a feedback pumping system where the feedback signal is the pressure at the exit of the detector: the control module reads the gas pressure at the exit and it opens or closes automatically the solenoid valve in order to keep always the same pressure inside the detector. A Mass Flow Controller controls the gas flow into the detector. Both the pressure and the gas flow can be set on the front panel of an electronic module (MKS 146).
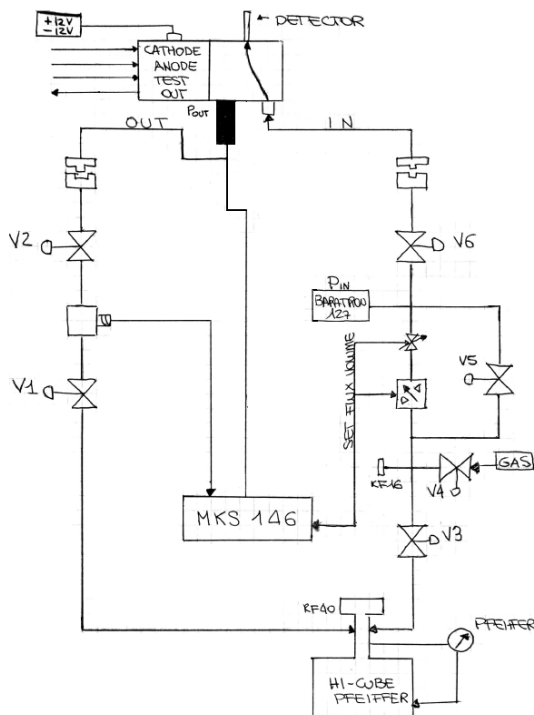

FIGURE 21 - SCHEME OF THE GAS FLOW AND VACUUM STATION AND PHOTO

The feasibility of constructing a sealed mini-TEPC will be discussed in this thesis. Larger TEPCs used as area monitors already work in sealed mode with a

periodic change of gas that depends on the TEPC dimensions and materials. Mini-TEPCs have a sensitive volume of 0.6 mm^3 and the quantity of gas inside the cavity is small, this means a faster contamination of the gas. Nevertheless, the possibility of working in gas-sealed mode would be a great simplification of the apparatus in order to be used in clinical environment.

Chapter 4

Data processing

The traditional analog pulse processing has been employed in this work. Pulses converted by three different analog-to-digital converters (ADC) produce three sub-spectra, which are processed and joint offline to obtain the whole microdosimetric spectrum.

4.1 Calibration in mV and re-binning

The three sub-spectra must be calibrated in mV. The first thing to do before starting a measure is to calibrate the electronic chain from channels of the ADC to mV. A high precision pulser (Model BNC PB-4) was used to verify the integral and differential linearity of each ADC and to establish the calibration curve (between channel number of the ADC and the voltage amplitude). Then, the three pulse height spectra measured with different electronic gains are merged off-line to obtain the whole pulse height spectrum. Afterwards, the linearly distributed data are re-binned into logarithmically spaced data. An example of the three sub-spectra with overlapping regions, after the channel to pulse-height calibration and the 10-log re-binning, is shown in Figure 22. The peak at the end of low-LET sub-spectrum is produced by signals that exceed the maximum pulse amplitude that the ADC converts (+10 V).

The three different sub-spectra collected by the ADCs are then re-binned in a logarithmic representation. The ascites axis is divided into D decades and N logarithmic intervals per decade that are then normalized in count density n (y) in compacted intervals. In each decade j, the number of intervals of h is:

$$y_{i+1}^{j} = y_i \cdot 10^{i/N} \hspace{2cm} \textbf{29}$$

while the width of the logarithmic interval is:

$$\Delta y_i = y_i \cdot (10^{1/2N} - 10^{-1/2N}) \qquad\qquad \textbf{30}$$

Where i = {0,…,D·N}, N=60.

The counts in each Δy_i are averaged in order to obtain the re-binned counts N_i. At the end of the re-binning procedure the three sub-spectra have a superimposition region that is a fundamental condition to join them together.
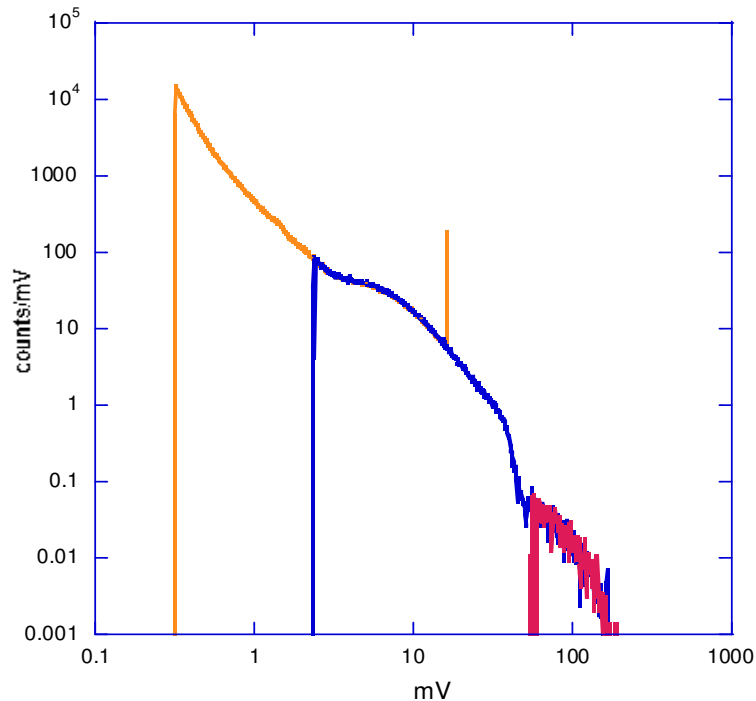
4.2   Joining procedure

After the calibration in mV and 10-log re-binning the sub-spectra have to be joined together. The black lines in the image below indicate the regions of best superimposition of the sub-spectra, the linearity of the superimposition region is checked calculating the compatibility coefficient of the slopes.
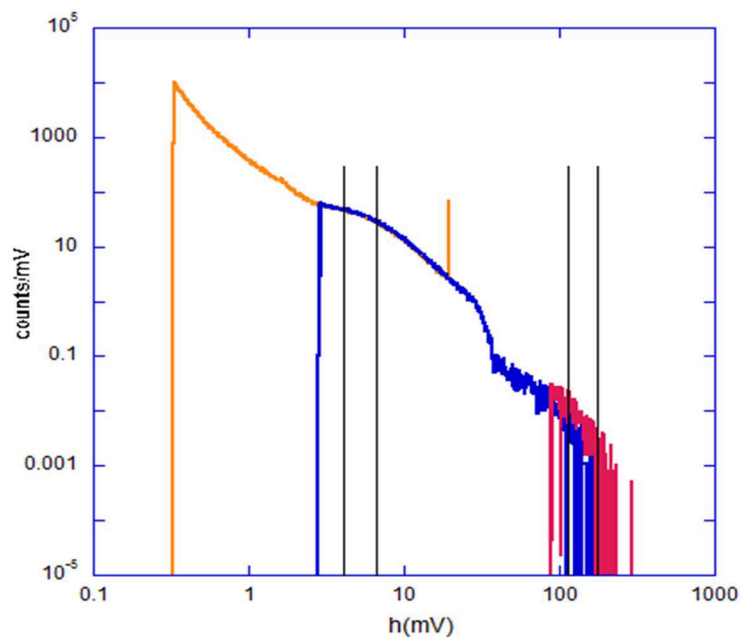
FIGURE 23 – INDIVIDUATION OF THE SUPERIMPOSING REGION IN ORDER TO JOIN THEM TOGETHER

After this check, the cutting point is calculated inside those regions as the central point in the region with the minimum variance calculated between the counts of the sub-spectra.

The next step is to convert the spectrum into a density distribution where f(y) is the frequency distribution and d(y) is the dose distribution of the lineal energy y. The conversion is possible through the following formulas:

$$f(y_i) = \frac{n(y_i)}{\sum_{y_0}^{y_{max}} n(y_i) \cdot \Delta y_i} \tag{31}$$

$$d(y_i) = \frac{y_i \cdot f(y_i)}{\sum_{y_0}^{y_{max}} y_i \cdot f(y_i) \cdot \Delta y_i} \tag{32}$$

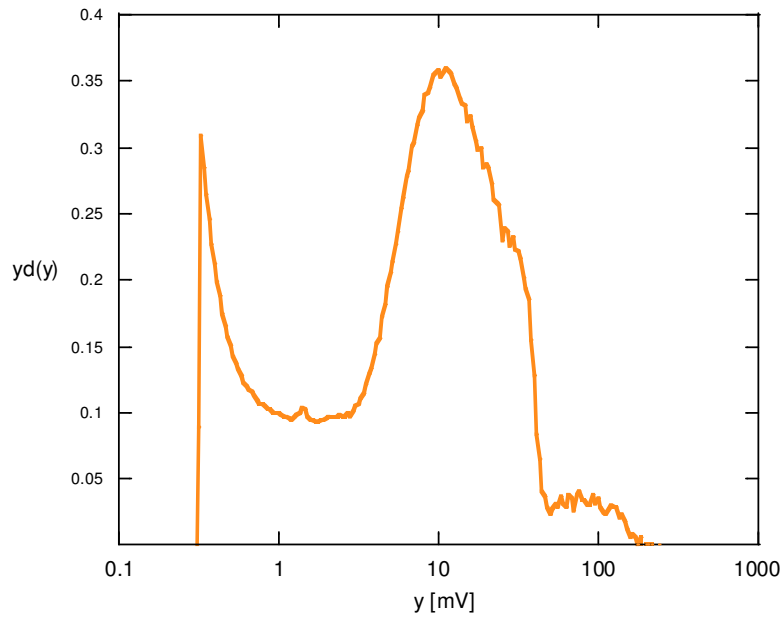The entire density distribution is normalized to the unity.

4.3 Calibration in energy and extrapolation

The last passage to do is the calibration in keV/µm and extrapolate the spectrum in order to not underestimate or overestimate the dose at low LET.

Two possible calibration techniques can be performed in TEPCs.

a) Alpha calibration

Commercial TEPCs are equipped with a built-in-α-particle source (^{244}Cm or ^{241}Am) for calibration purposes. There are several uncertainties associated with this calibration technique that reach the order of 10% while the maximum uncertainty accepted in the clinical environment is 5%. The main sources of uncertainties are:

- Usually the effective energy of the α-particle is less than the nominal energy due to self-absorption (5%)
- The α-particle has to be evaluated from tabulated data but discrepancies between stopping power data are present (4%)
- The unknown details of the geometrical path of α-particle.

b) <u>Edge technique</u> [V. Conte, 2013]

If the internal source is not available or cannot be used because of its uncertainties, an external radiation field must be used in order to calibrate spectra. The edge technique is based on the identification of marker points specific of a particular radiation field.

In a gamma source field, the particular characteristic of the spectrum is the so-called electron edge that is due to the electrons that stop exactly at the end of the sensitive volume, they are called "*exact stoppers*", which release the maximum of the lineal energy in the cavity.

In a proton or neutron field, it is easy to recognize the proton edge that corresponds to the maximum of the energy imparted by protons in the cavity if we can assume that they are all crossers. This assumption is correct in the simulate site of 1 μm TE, while in the simulate site size of 1.2 μm TE the proton edge is due to the exact stoppers.

This second calibration technique consists of two steps: one or more marker points are identified in the measured spectrum and then, analysing the specific feature of the microdosimetric spectrum, a value of lineal energy is assigned to those marker points for each radiation field.

To identify the marker point reducing the uncertainties due to the fitting interval and the low statistics Conte *et al.* proposed a Fermi-like function, the function is:

$$hd(h) = \frac{A}{1+e^{B(h-C)}}$$

33

C has the same dimensions of h and it identifies the position of the function inflection point (C=h_{flex}), in this point hd(h)=A/2. The parameter B represents the steepness of the function around the inflection point. By fitting the edge with a Fermi-like function, it is possible to identify three marker points:

$$h_{flex} = C; \qquad h_{\delta\delta} = \frac{\ln(2+\sqrt{3})}{B} + C; \qquad h_{tc} = \frac{2}{B} + C$$

34

The first marker point is the x value of the inflection point, the second one represents the x value in which the second derivative reaches its maximum and the last one is the intercept of the tangent through the inflection point with the x-axis. It

has been demonstrated [V. Conte, 2013] that h_{tc} is the most precise marker point with an uncertainty smaller than 0.5% in high statistics (10^6 events) and its position is almost invariant with fitting range and deviations from the mean value are 0.1% at maximum.

Once the marker points are identified, the appropriate values of lineal energy must be assigned to them experimentally.

For gamma rays radiation fields the assignment was performed with a large TEPC calibrating the pulse height with an internal ^{244}Cm α-particle source and in order to transfer the calibration for α-particles to photons the ratio W_{el}/W_α=0.964 was applied. Experimental values of the marker points have been assessed in function of the simulated diameter with the following results:

$$\frac{y_{flex}}{\frac{keV}{\mu m}} = 10.4 \cdot \left(\frac{D}{\mu m}\right)^{-0.29} \quad \frac{y_{\delta\delta}}{\frac{keV}{\mu m}} = 13.8 \cdot \left(\frac{D}{\mu m}\right)^{-0.40} \quad \frac{y_{tc}}{\frac{keV}{\mu m}} = 15.5 \cdot \left(\frac{D}{\mu m}\right)^{-0.43}$$

35

These equations can be used to calibrate mini-TEPCs simulating volumes from 0.3 µm to 2.3 µm using an external ^{137}Cs gamma-ray source.

Among the three markers the intercept of the tangent through the inflection point is the most precise one with respect to statistics and fitting intervals, while the inflection point is the less sensitive to D and pressure variations probably because it is approximately completely determined by the mean value of energy transfer along the maximum path length. The other two marker points, $y_{\delta\delta}$ and y_{tc}, include the parameter B which is related to the energy-loss straggling of electrons.

In the analysis of the experimental data, the electron-edge technique was employed giving the value of 15.5 keV/µ to the intercept with the x-axis of the tangent through the inflection point. While in the spectra acquired in neutron radiation field the proton edge was used. The marker point to recognised as the most precise one is the inflection point to which a value of 150 keV/µm was assigned both for the simulate site of 1 µm TE and 1.2 µm TE because according to the ICRU table the stopping power can be assumed within the uncertainties (5-10%) [ICRU 49, 1993].
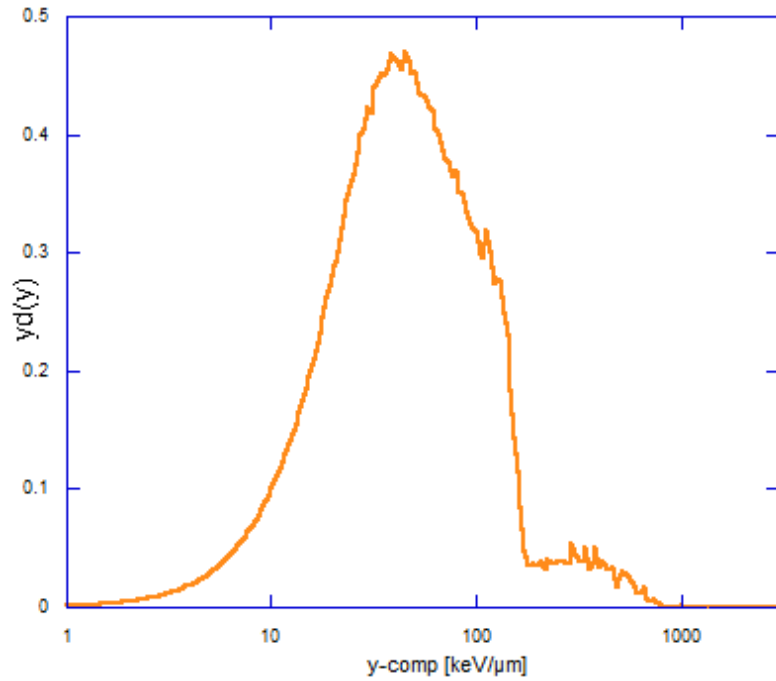
FIGURE 25 - FINAL SPECTRUM CALIBRATED WITH THE PROTON EDGE TECHNIQUE IN KEV/UM

The lower threshold of the measurement depends on the noise level. To have a complete spectrum an offline linear extrapolation is performed.

Chapter 5

<u>Measurements and analysis</u>

The aim of the measurements performed in this thesis with the mini-TEPC AMiCo 7 was twice.

First aim is to study in detail the possible non-linear response of the detector with high LET radiations. This behaviuor was observed for the first time by Elisa Motisi (2015) with a similar mini-TEPC, basically a copy called AMiCo 6. A systematic characterization of the response of the detector at different working voltages was done. For these measurements, both a ^{137}Cs gamma-ray source of 1.1 GBq and the fast neutrons of the ^{7}Li(d,n)^{8}Be reaction have been used.

The second aim is to perform a preliminary test of the detector response in sealed modality, that means without flowing the counting gas into the mini-TEPC. For these measurements, a ^{137}Cs gamma-ray source of 1.1 GBq emitting 662 keV gamma-rays was used.

5.1   Mini-TEPC response at different applied voltage

Measurements were performed in propane gas at 454 mbar and 544 mbar of pressure, corresponding to 1 μm and 1.2 μm site size in propane-TE gas (the tissue-equivalent gas-mixture based on propane) at 1 g/cm^3 of density respectively. All the measurements were performed in gas flow modality.

5.1.1 Mini-TEPC response to ^{137}Cs gamma rays at 1μm site size

Measurements have been performed positioning the mini-TEPC in the front of the gamma irradiator hole (see figure 26). Measurements were performed in standard way (see chapter 4). The multichannel analyser (MCA) has been calibrated in volt by using a research pulser. Two sub-spectra have been enough to construct the full microdosimetric spectrum off-line.

FIGURE 26 – THE GAMMA SOURCE IRRADIATOR AND THE MINI-TEPC. THE GAMMA BEAM EMERGES FROM THE SMALL HOLE BEHIND THE DETECTOR
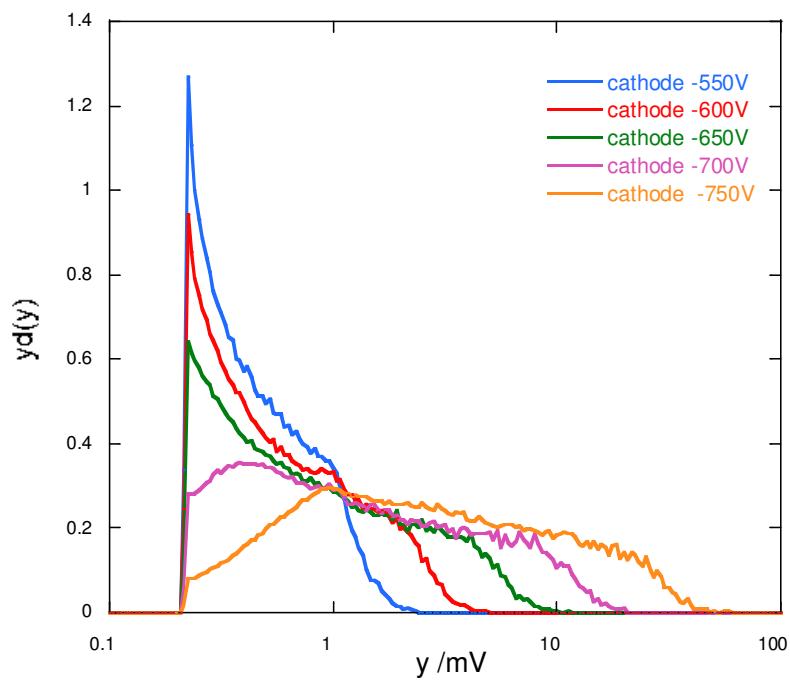

FIGURE 27 – MICRODOSIMETRIC SPECTRUM OF [137]CS GAMMA SOURCE AT DIFFERENT APPLIED VOLTAGES AT THE CATHODE WALL

In figure 27 the voltage-calibrated microdosimetric spectra of ^{137}Cs gamma source are plotted at different applied voltages. The cathode wall has been biased with a negative voltage, being the anode wire earthed through the charge pre-amlifier. The smallest detected pulse-size is 0.2 mV. The figure shows an increase of pulse

44

sizes with ∆V because of the gas gain factor increase. To better quantify such an increase, the electron-edge has been properly procecessed (see chapter 4).

Figure 28 shows the logarithm of the intercept with the 0X axis of the tangent through the e-edge inflection point [V. Conte, 2013]. This parameter has been taken as representative of the e-edge, hence of the gas gain. It can be used to study the gas gain change with the volatage difference between cathode and anode (∆V).
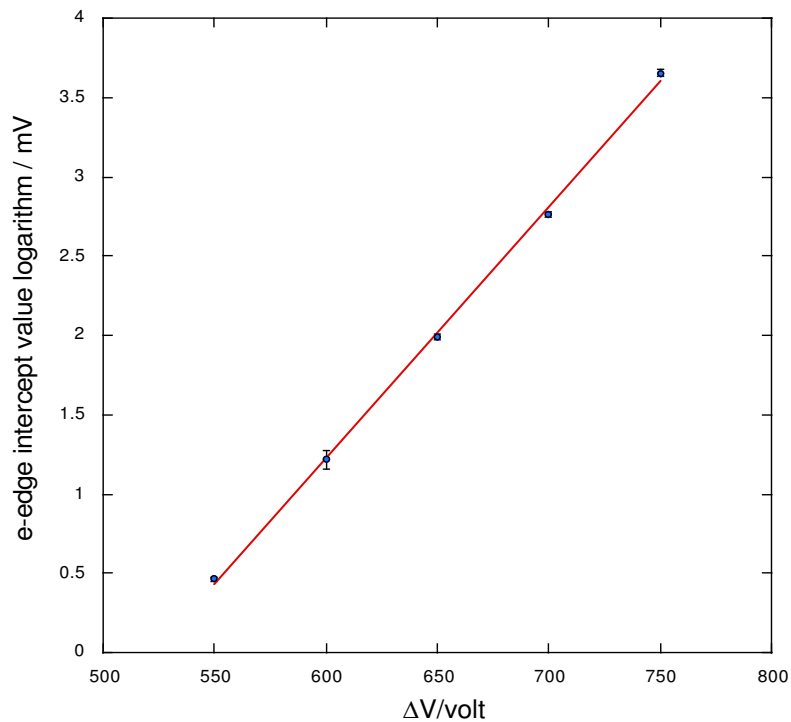

FIGURE 28 – LOGARITHM OF THE E-EDGE VALUE (SEE TEXT) AGAINST THE VOLTAGE DIFFERENCE ∆V (BLACK DOTS). LINEAR BEST-FIT OD DATA (RED LINE)

Since the gas gain is in first approximation an exponential function of ∆V (§2.5.1), the pretty good linearity of the gas-gain logarithm (namely the intercept with 0X axis of the e-edge inflection tangent) shows that not-linear phenomena in this range of applied voltages do not affect the mini-TEPC response.
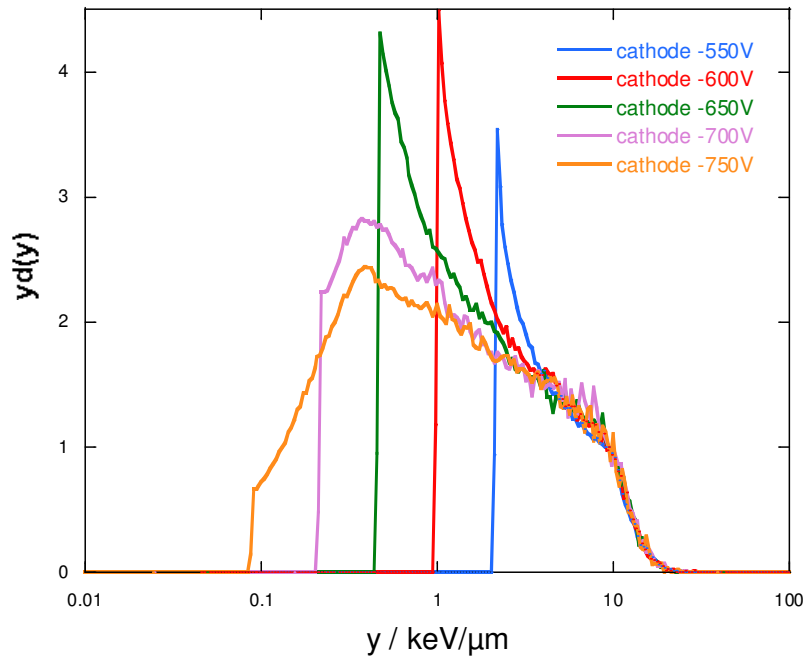
Figure 29 shows the microdosimetric spectra of figure 27 after lineal energy calibration. The calibration has been performed assigning the lineal energy value of 15.5 keV/µm to the intercept with 0X axis of the e-edge inflection tangent [V. Conte et al., 2013]. The spectra shapes for relatively large pulses (y > 4 keV/µm) superimpose well. On the contrary, the lowest detection threshold (LDT) is rather different. At ΔV = 550 V, LDT ≈ 4 keV/µm, which means an event of ≈ 100 electrons. Smaller events are spoiled by the electronic noise. At ΔV = 750V, LDT ≈ 0.09 keV/µm, which means an event of ≈ 2 electrons.

The charge pre-amplifier used during the measurement is home made. It has low noise (300 electrons equivalent) and large dynamic range (4 and ½ order of magnitude). In order to test whether the charge pre-amplifier performances depend on the anode voltage, the measurement at ΔV = 750 V was repeated dividing the voltages between anode and cathode.

Figure 30 show three spectra, all of them collected with ΔV = 750 V, but with an anode voltage of 0 V, +100 V, +350 V respectively. Any difference appears among the three spectra.

Data point out the mini-TEPC response to gamma rays does not depend on applied voltage (for ΔV ≤ 750 V) and voltage sharing between anode and cathode. This finding could be valid only for relatively small pulses. In fact, taking into account that

the gas gain factor is ~ 1000 at 750 V, the electronic avalanche inside the mini-TEPC is always $<\approx 10^6$ electrons, when gamma rays are detected.

In the following will be studied the mini-TEPC response to larger events, namely to high-LET radiations, which can give rise to electronic avalanches hundred times larger.
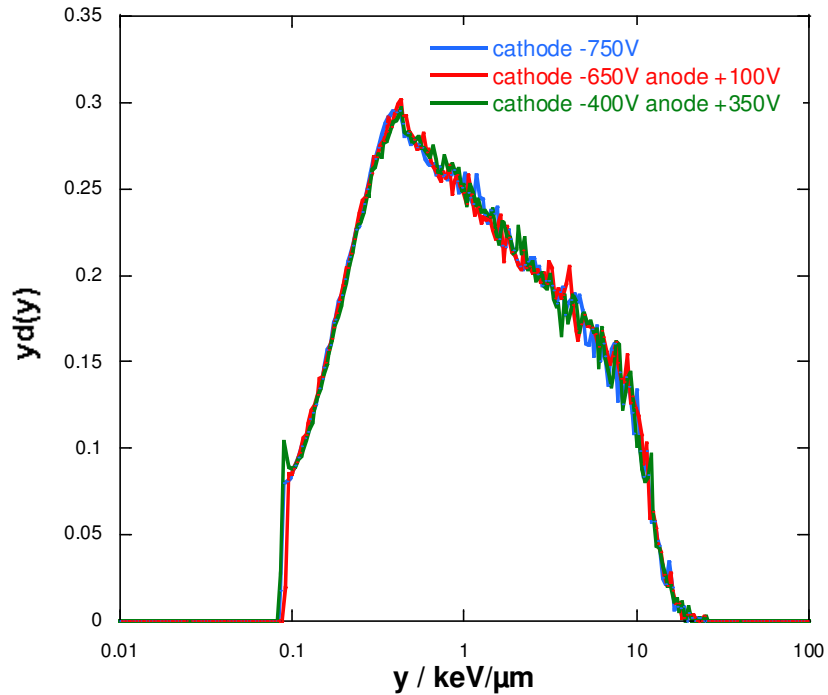

FIGURE 30 - SHAPE COMPARISON DIVIDING THE VOLTAGE DIFFERENCE BETWEEN ANODE AND CATHODE IN DIFFERENT WAYS IN LOW LET RADIATION (750 V)

5.1.2 Mini-TEPC response to fast neutrons at 1 µm simulated size

High-LET radiation field has been produced by using the reaction $^7Li(d,n)^8Be$, which has a Q-value of 15.1 MeV. A deuteron beam of 5 MeV has been used together wth a LiF target 1000 µg/cm² thick. Therefore, fast neutrons emerging fron the reaction have a continuous spectrum between 15 and 20 MeV, The detector was positioned at 1 centimetre far from the target (see figure 31). The beam intensity was 100 nA. The count was between 6 kHz (750 V) and 400 Hz (550 V) depending on the detection threshold, which in turn is due to the voltage applied. Since the noise at the CN accelerator was high, it was not possible to accurately measure y events less than ~ 1 keV/µm.
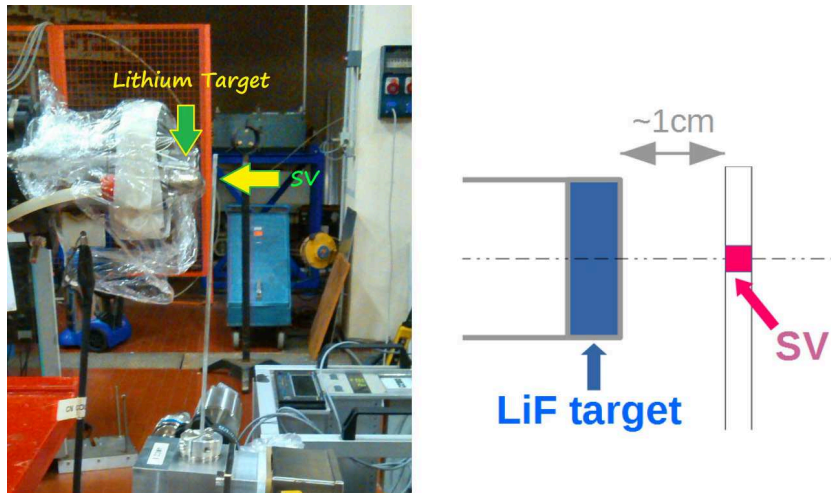
FIGURE 31 – LEFT SIDE: THE MEASUREMENT POINT AT THE CN ACCELERATOR OF LNL. RIGHT SIDE: OUTLINE OF THE IRRADIATION GEOMETRY

Spectra were measured in propane gas without changing detector position and the deuterion beam features. Only the applied voltage at the cathode has been changed from -550 V to -750 V.
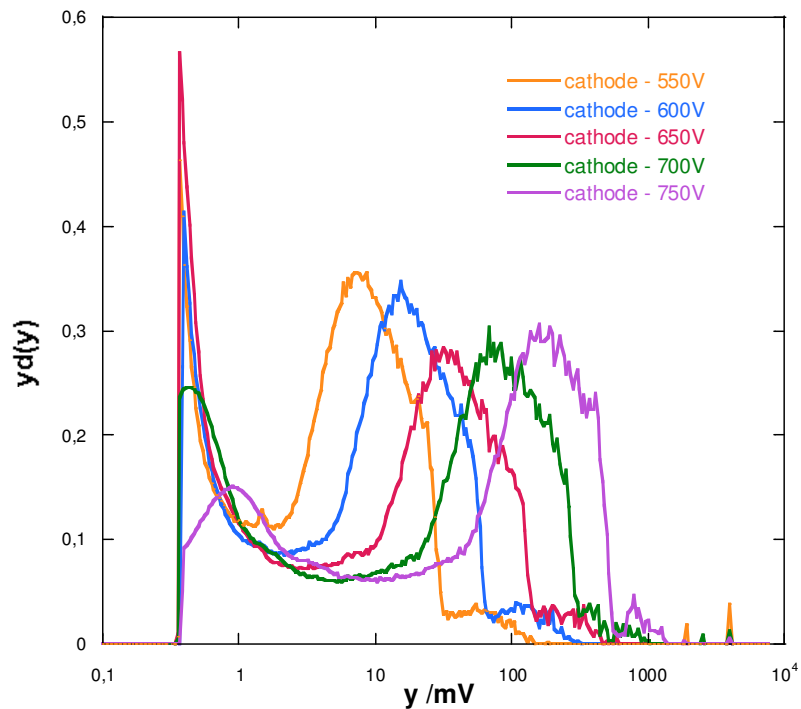

FIGURE 32 – MICRODOSIMETRIC SPECTRUM OF FAST NEUTRONS (SEE TEXT) IN 1 µM SITE AT DIFFERENT APPLIED VOLTAGES AT THE CATHODE WALL

In figure 32 the voltage-calibrated microdosimetric spectra of fast neutrons are plotted at different applied voltages. The cathode wall has been biased with a negative voltage, being the anode wire earthed through the charge pre-amlifier. Measurements have been performed in propane gas at 1 μm propane-TE equivalent size (when scaled at 1 g/cm^3 density). The smallest pulse-size in figure is ~ 0.4 mV. However, spectra are affected by backgound noise distorsions up to more than 1 mV. Similarly to gamma measurements, the figure shows an increase of pulse sizes with ΔV because of the gas gain factor increase. To better quantify such an increase, the proton-edge (p-edge), namely the sharp decrease after the large main peak, has been properly procecessed (see chapter 4).

Figure 33 shows the logarithm of the inflection point of p-edge.This parameter has been taken as a better representative of the p-edge, since it minimizes the contribution of larger events, which are not due to protons
The gas gain, namely the p-edge inflection point, follows a linear trend with the applied ΔV voltage, similarly to the e-edge of gamma rays (see § 5.1.1). However, the linear best-fit of the four first data points out that at highest voltages the gas gain could not follow anymore a linear trend with ΔV.
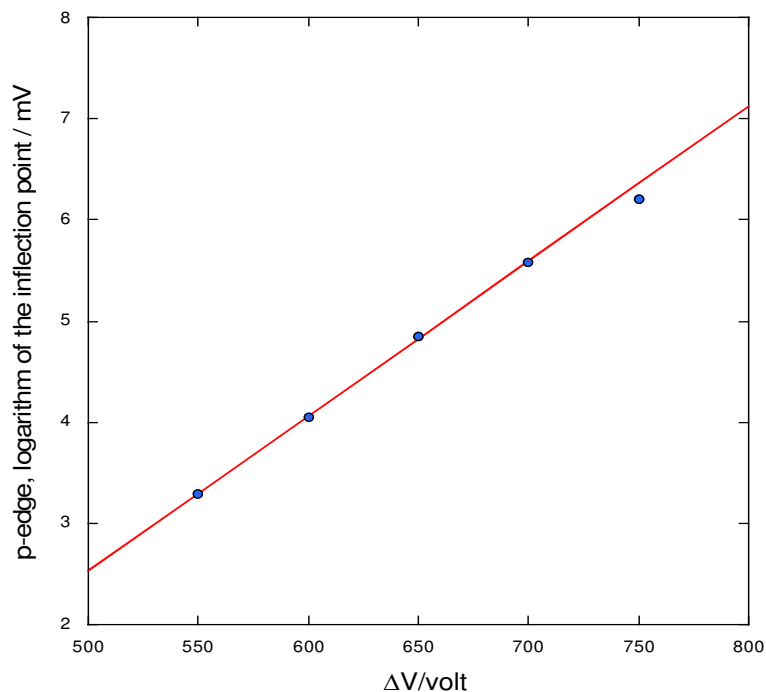

FIGURE 33 – BLACK DOTS: LOGARITHM OF THE P-EDGE VALUE (SEE TEXT) AGAINST THE VOLTAGE DIFFERENCE ΔV. RED LINE: LINEAR BEST FIT OF THE FOUR FIRST DATA (UP TO 700 V)

The inflection point of the p-edge gas has also been used for lineal energy calibration. The value of 150 keV/μm has been taken for the proton edge value, namely the maximum stopping power in propane-TE gas multiplied by 3/2.

Figure 34 shows the fast neutron microdosimetric spectra calibrated in lineal energy. Spectra have been cut at 2 keV/μm, since smaller events were affected by electronic noise. In order to improve spectra comparison, the yd(y) value have been scaled to obtain 1 for the main peak (proton peak) value.

Figure 34 shows that:

i)   the light-ion events (y > 150 keV/μm) shift towards lower y values with ΔV increase;

ii) at ΔV = 750 V the proton peak appears distorted, possibly because of the upper-mentioned light-ion event shift; this distortion could be the reason of the observed loss of gas gain linearity at high ΔV values (see figure 33);

iii) at ΔV = 550 V the light-ion pulses are well separated by the proton edge, however the low y events (y < 10 keV/μm) are distorted, possibly because of the electronic noise.
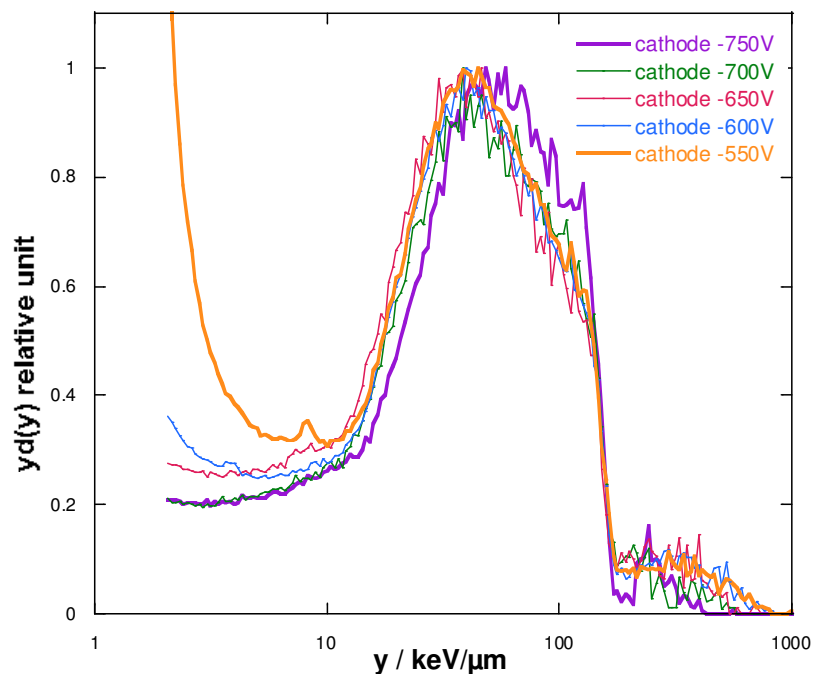

FIGURE 34 – SPECTRA OF FIGURE 32 AFTER LINEAL ENERGY CALIBRATION (SEE TEXT). THE YD(Y) VALUES ARE SCALED TO THE MAIN PEAK MAXIMUM VALUE

Because of the tiny size of the mini-TEPC, as well as the pulse processing of the front-end electronics, its response could be affected also by the voltage value of one electrode. Therefore, we have compared microdosimetric spectra with the same ∆V value, but with different voltage sharing between anode and cathode.

Figure 35 shows five spectra, all of them collected at ∆V = 750 V, but with different electrode bias: the full voltage (positive) to the anode; the full voltage (negative) to the cathode and intermediate situations. We have already observed that at ∆V = 750 V and cathode voltage – 750 V, the light-ion spectral component shifts towards lower y-values.

The figure shows:

i) the light-ion spectral component does not change giving to the anode a positive voltage;

ii) giving an increasing positive voltage to the anode increases the low-y part of the proton peak, deforming the microdosimetric proton component.
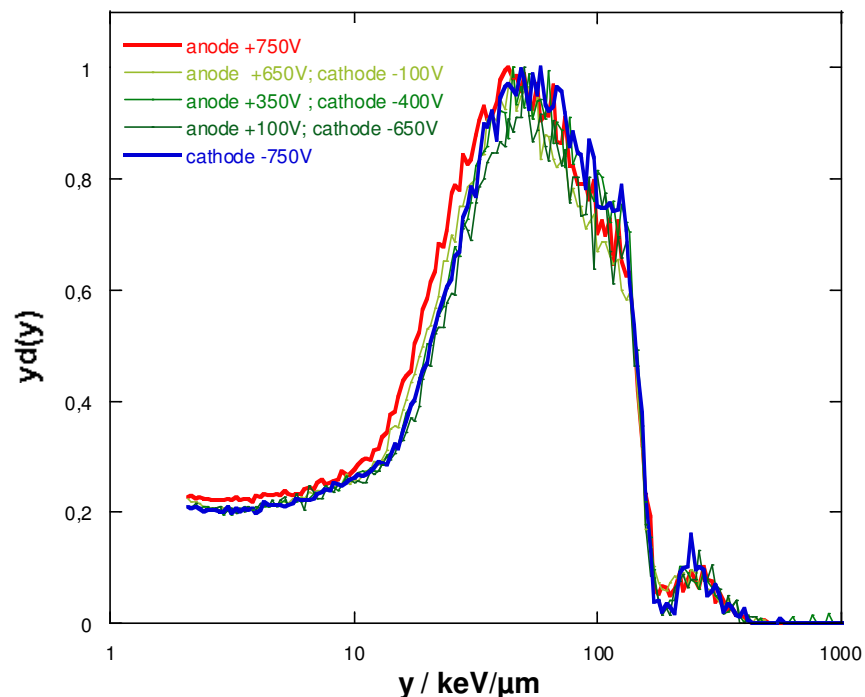

FIGURE 35 – MICRODOSIMETRIC SPECTRA AT ∆V=750 V WITH DIFFERENT VOLTAGE SHARING BETWEEN THE ANODE AND CATHODE

Figure 36 shows four spectra all of them collected at $\Delta V = 600$ V, but with different electrode bias: the full voltage (positive) to the anode; the full voltage (negative) to the cathode, one intermediate situation and a negative voltage bias to the anode. We have already observed that at $\Delta V = 600$ V and cathode voltage - 600 V, the light-ion spectral component is well separated from the proton component, moreover the all the spectrum is fully consistent with literature data.

The figure shows:

i) giving an increasing positive voltage to the anode strongly increases the low-y part of the spectrum, making unreliable the microdosimetric spectrum for y < 10 keV/μm;

ii) with the anode biased at high positive voltage pulses appear at high y-values, which have not physical meaning being over the maximum pulse size due to light ions set in motion by the fast neutrons;

iii) biasing the anode with a negative voltage decreases the electronic noise and possibly improve the spectrum quality of the reference spectrum with the anode earthed.
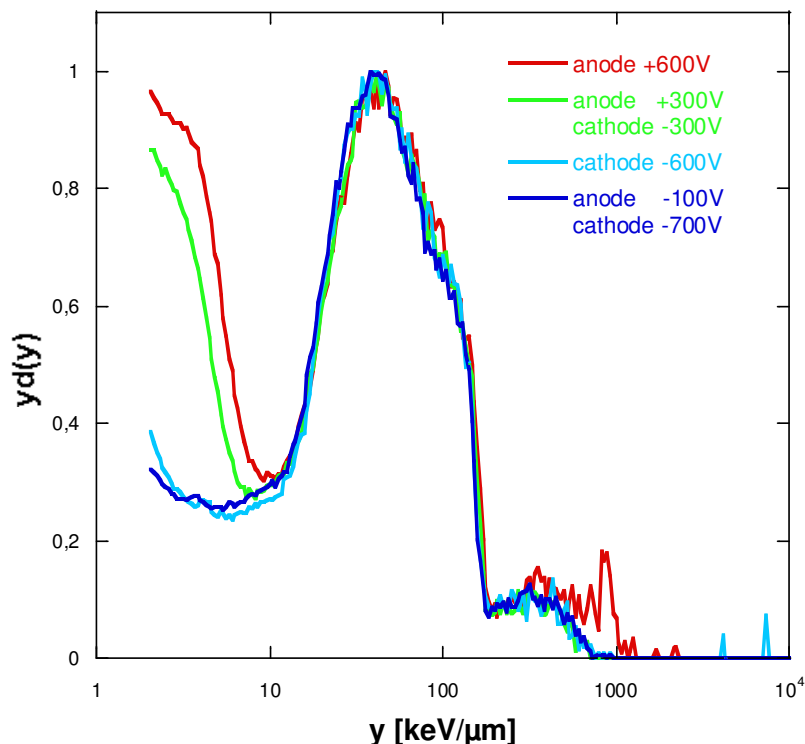

FIGURE 36 – MICRODOSIMETRIC SPECTRA AT ΔV=600 V WITH DIFFERENT VOLTAGE SHARING BETWEEN THE ANODE AND CATHODE

5.1.3 Mini-TEPC response to fast neutrons at 1.2 μm simulated size

The following spectra were obtained in the same neutron radiation field of those at 1 μm but in a different day, in this case the equivalent propane-TE site diameter is of 1.2 μm that corresponds to a pressure of 544 mbar of propane gas.

In figure 37 the voltage-calibrated microdosimetric spectra are plotted at different applied voltages. The cathode wall has been biased with a negative voltage, being the anode wire earthed through the charge pre-amlifier. ΔE values have been chosen to obtain the reduced electrical field at the anode surface as for measurements at 1μm simulated diametre. The smallest pulse-size in figure is ~ 0.3 mV. However, spectra are affected by backgound noise distorsions up to more than 1 mV. Similarly to neutron measurements at 1 μm site, the figure shows an increase of pulse sizes with ΔV because of the gas gain factor increase. To better quantify such an increase, the proton-edge (p-edge) has been properly procecessed (see chapter 4).
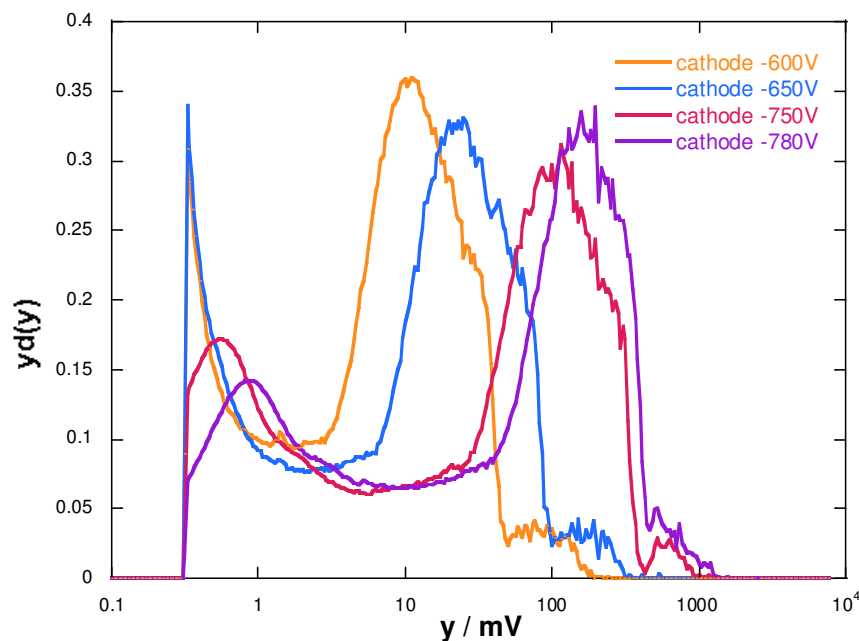

FIGURE 37 - MICRODOSIMETRIC SPECTRUM OF FAST NEUTRONS IN 1.2 μM SITE AT DIFFERENT APPLIED VOLTAGES AT THE CATHODE WALL

The gas gain, namely the p-edge inflection point, follows a linear trend with the applied ΔV voltage up to 750 V. At higher ΔV value (780 V) the gas gain, namely the p-edge inflection point, is smaller as expected, as for 1 μm site measurements (see figure 33).
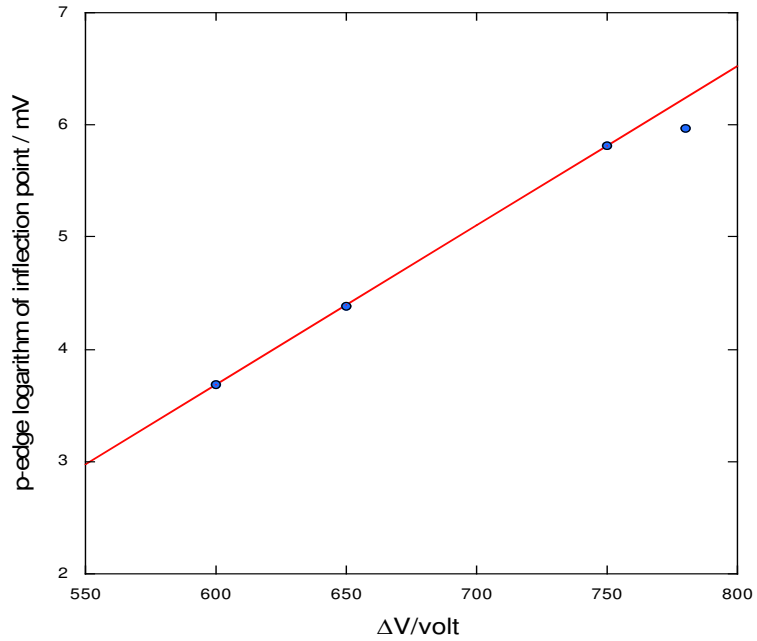
Similarly to figure 34, the inflection point of the p-edge gas has also been used for lineal energy calibration. The value of 150 keV/μm has been taken for the proton edge value as for 1μm measurements.
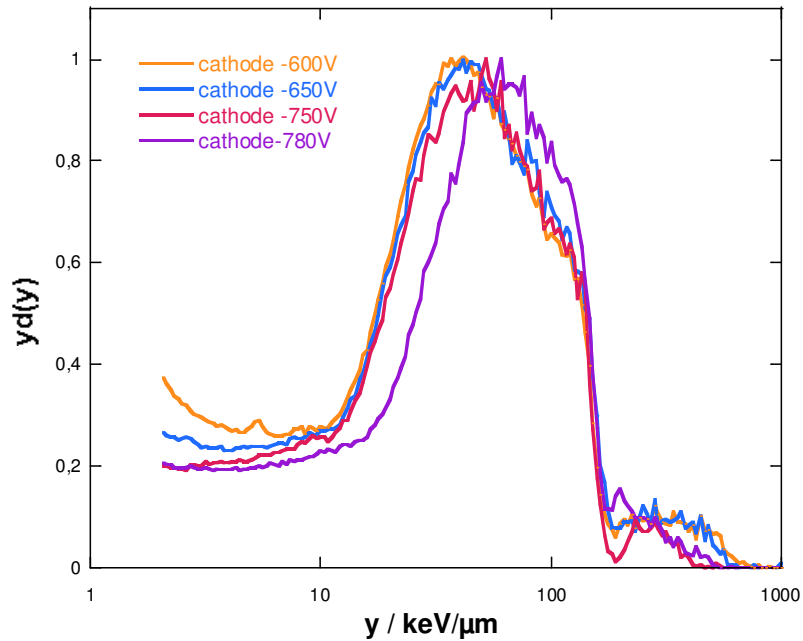

FIGURE 39 - SPECTRA OF FIGURE 37 AFTER LINEAL ENERGY CALIBRATION (SEE TEXT). THE YD(Y) VALUES ARE
SCALED TO THE MAIN PEAK MAXIMUM VALUE

Figure 39 shows the fast neutron microdosimetric spectra calibrated in lineal energy. Spectra have been cut at 2 keV/µm, since smaller events were affected by electronic noise. In order to improve spectra comparison, the yd(y) value have been scaled to obtain 1 at the main peak (proton peak) value.

Figure 39 shows that:

i)   the light-ion events (y > 150 keV/µm) shift towards lower y values with ΔV increase, as already seen at 1 µm;

ii)   at $V_{cathode}$ = - 780 V the proton peak appears distorted, similarly to the spectrum at 1 µm and $V_{cathode}$ = - 750 V; this distortion could be the reason of the observed lost of gas gain linearity at high ΔV values (see figure 38);

iii)   the spectrum at $V_{cathode}$ = - 650 V is similar to the 1 µm spectrum at $V_{cathode}$ = -650 V, although the reduced electrical field at the anode surface is equal to that one at $V_{cathode}$ = - 550 V. This finding suggests that the spectral distortion at low y-values depends on the low cathode absolute-voltage rather than on the low gas gain, namely the low reduced electrical field at the anode surface.

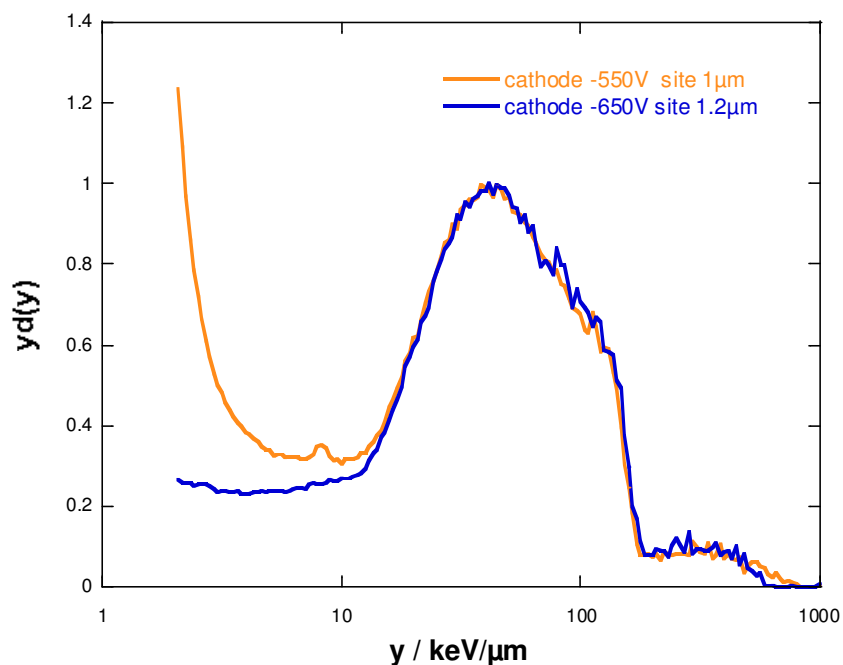## 5.1.4   Mini-TEPC response comparison at different simulated site sizes

FIGURE 40 - NEUTRON MICRODOSIMETRIC SPECTRA AT TWO DIFFERENT SITE SIZES AND LOW REDUCED ELECTRICAL FIELD. YD(Y) VALUES ARE RELATIVE THE PROTON PEAK MAXIMUM

Figure 40 compares directly the spectrum collected at 1 μm with that one collected at 1.2 μm, being the reduced electrical field at the anode surface, hence approximately the gas gain, the same. As already observed, the spectral distortion at 1 μm site for y-value < 10 keV/μm is not visible in the 1.2 μm site. The figure shows also that a small yield of light-ion events with > 550 keV/μm disappears in the 1.2 μm measurements. This phenomenon points out that some light ions, already "crossers" in 1μm site, become "stoppers" in 1.2 μm site (see figure 16 of § 2.5.4).
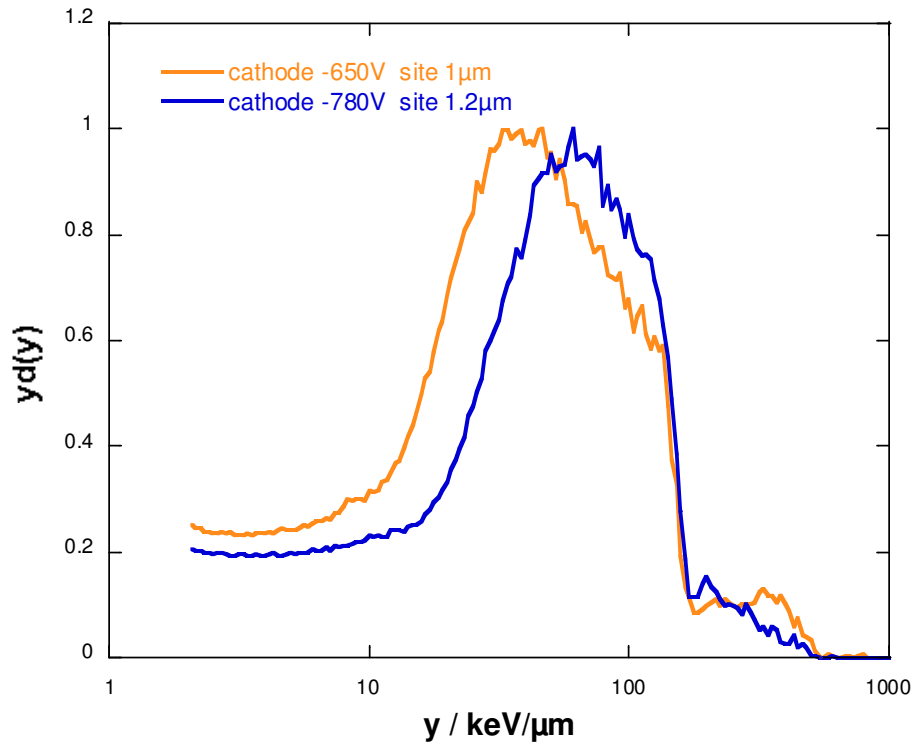
FIGURE 41 - NEUTRON MICRODOSIMETRIC SPECTRA AT TWO DIFFERENT SITE SIZES AND HIGH REDUCED ELECTRICAL FIELD. YD(Y) VALUES ARE RELATIVE THE PROTON PEAK MAXIMUM

Figure 41 compares directly the spectrum collected at 1 μm with that one collected at 1.2 μm collected at higher gas gain (namely higher reduced electrical field) with respect the measurements of figure 40. The spectrum at 1.2 μm appears strongly distorted with respect that one at 1 μm. That makes evident what has been already observed in figure 39 and 40, that is high absolute-voltage values at the electrodes deform microdosimetric spectra, even if the gas gain is relatively small.

5.2 Mini-TEPC response in sealed conditions

Before measurements, the detector was conditioned. It has been left in vacuum for three days to clean the sensitive volume from the impurities. After these days of vacuum three cleanings with propane were done with the following procedure: it was filled with propane, left in flux mode and then put in vacuum again. The aim was to saturate the plastic walls of propane, in order to minimise outgassing contamination while measuring. After this week of conditioning, the gas-flow and vacuum station (see figure 21) was isolated from the mini-TEPC by closing the gas-input and gas-output valves. Measurements were performed by using the ^{137}Cs source and the gamma irradiator (see figure 26). All the measurements have been performed giving to the cathode wall - 750 V of electrical potential, being the anode wire earthed through the pre-amplifier. All the measurements have been performed at 1 μm propane-TE equivalent site size, namely with propane gas initially set at 454 mbar of pressure (at 20 °C). In order to check the pressure drift due to degassing phenomena, the counting gas pressure was measured, through the MKS absolute gas-pressure transducer inserted in the mini-TEPC support, before any measurement.

Microdosimetric data have been processed in standard way, see chapter 4. In particular, only two sub-spectra have been used because of the reduced dynamic range of pulses. The electron-edge value was assessed by using the Fermi-like best fit and the intercept with the 0X-axis of the tangent through the inflection point. In table 1 time of measurement, gas pressure and electron edge value are shown.

TABLE 1 - TEST IN SEALED MODE, THE ELECTRON EDGE IS REPRESENTED BY THE INTERCEPT OF THE TANGENT THROUGH THE INFLECTION POINT WITH THE 0X-AXIS

TIME	PRESSURE	ELECTRON EDGE [mV]
0 hours	454.0±0.1mbar	39±1
71 hours	460.2±0.1 mbar	34.8±0.7
90 hours	458.8±0.1 mbar	29.2±0.4
96 hours	460.0±0.1 mbar	29.0±0.5
102 hours	460.0±0.1 mbar	29.4±0.3
106 hours	460.0±0.1mbar	28.7±0.4
126 hours	462.0±0.1 mbar	29.7±0.3
151 hours	465.8±0.1 mbar	28.4±0.3

Figure 42 shows microdosimetric spectra at increasing time after the detector sealing. Pulse spectra have been calibrated in volt by using a precision research pulser (see chapter 4). At first glance, the electron edge decreases towards lower values in the first hours, to remain constant in the following. To better analyse such shift, figure 43 shows the electron edge against the time. That shift points out a fast gas gain decrease of ~25% in the first 90 hours, followed by an almost constant behaviour (less than 3% shift) in the following 60 hours.
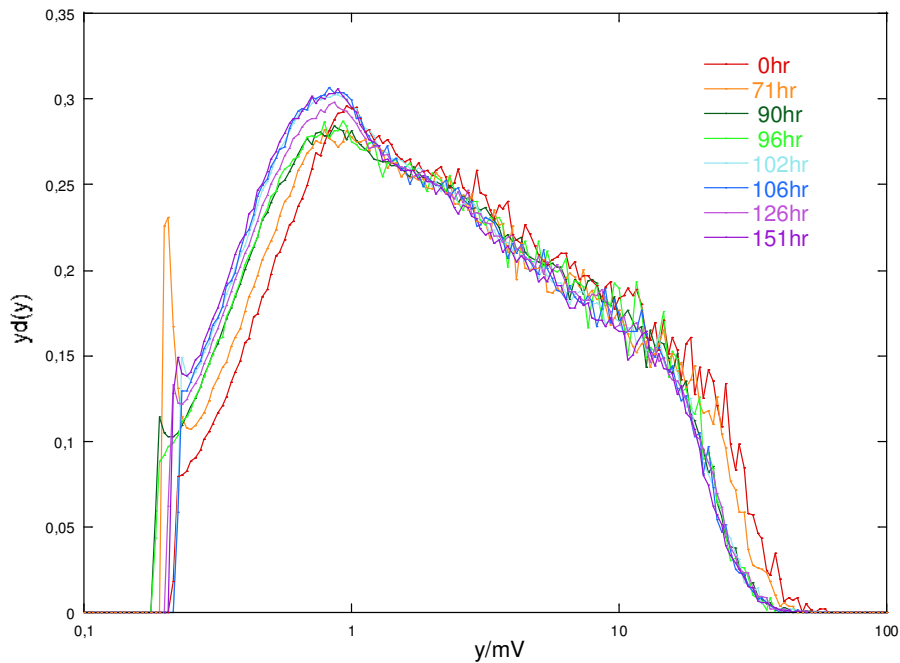

FIGURE 42 – ^{137}CS MICRODOSIMETRIC SPECTRA AT DIFFERENT TIMES AFTER THE MINI-TEPC SEALING

In figure 43 is also plotted the inverse of the pressure value (1/P) inside the mini-TEPC in relative values. Assuming that the gas gain is, for small variations, proportional to the reduced electrical field, hence proportional to 1/P, figure 43 tells us that the strong e-edge decrease in the first hours cannot be due to gas pressure increase inside the mini-TEPC. The gas pressure increase can instead explain the small gas gain decrease after 90 hours. The fast gas gain decrease after the counter sealing could be due to the quick gas contamination caused by plastic degassing. Such a degassing is quantitatively small (the gas pressure increases of less than 1%), but it can possibly poison the counting gas with electron-capturing molecules, from here the strong gas gain reduction.
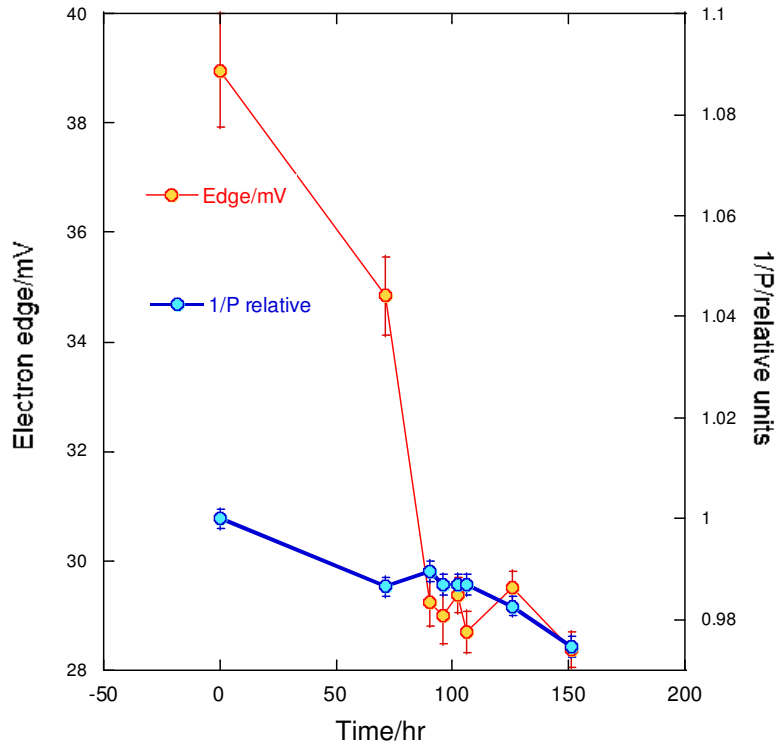
FIGURE 43 – RED CIRCLES: ELECTRON EDGE VALUES OF SPECTRA OF FIGURE 42 AT DIFFERENT TIMES AFTER THE MINI-TEPC SEALING. BLUE CIRCLES: INVERSE PRESSURE VALUES INSIDE THE MINI-TEPC, IN RELATIVE UNITS
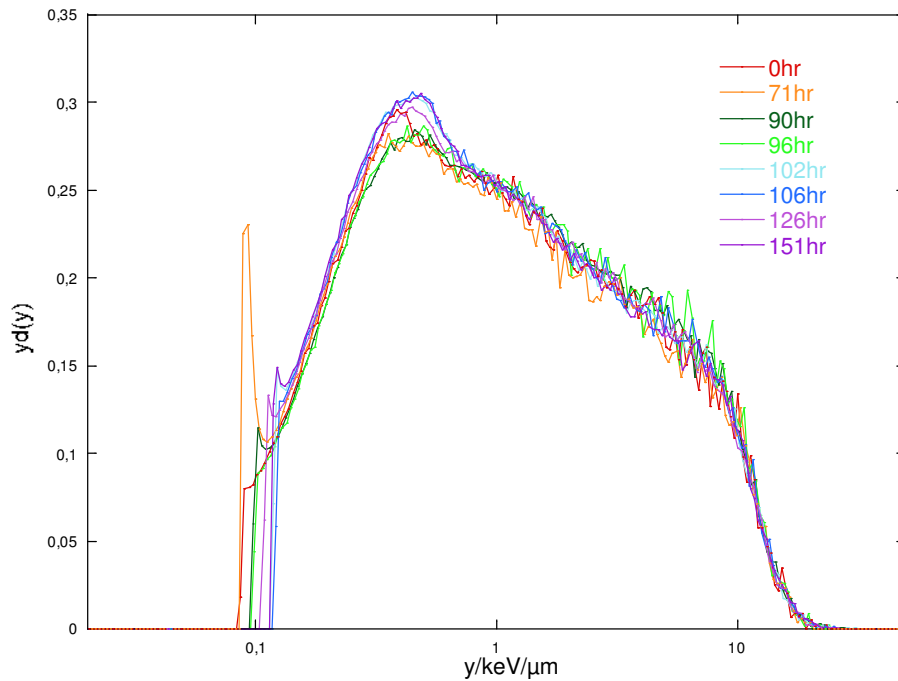

FIGURE 44 – MICRODOSIMETRIC SPECTRA OF FIGURE 44 CALIBRATED IN LINEAL ENERGY. TO FACILITATE THE COMPARISON, THE LOWER THRESHOLD HAS BEEN SET AT 0.14 KEV/μM FOR ALL THE SPECTRA

Figure 44 shows the same microdosimetric spectra of figure 42 after lineal energy calibration with the electron edge (see chapter 4). Inside the statistical fluctuations, the spectra shape does not change with the time increase, but for a group of events, between 0.3 and 0.6 keV/µm, the relative number of which increases lightly with time. The reason of such increase is not easily understandable. Further measurements are necessary to confirm such increase.

The invariance of spectral shape can be better assessed calculating the frequency-mean lineal energy ($\bar{y}_F$) and the dose-mean lineal energy ($\bar{y}_D$). Figure 45 and table 2 show the variation of the two averages with time (in the figure they are written Yf and Yd respectively). The uncertainty plotted in the figure (3%) is mainly due to the W-value uncertainty, being the intercept-value uncertainty less than 1%.
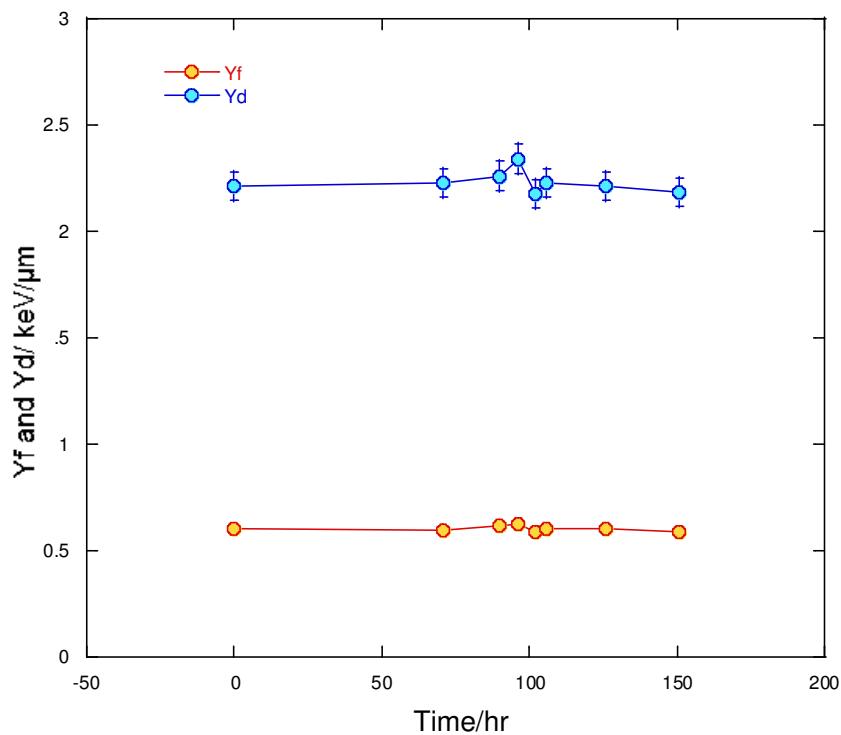
FIGURE 45– FREQUENCY-MEAN LINEAL ENERGY (YF) AND DOSE-MEAN LINEAL ENERGY (YD) OF SPECTRA OF FIGURE 44

TIME	$\bar{y}_F$ keV/µm	$\bar{y}_D$ keV/µm
0 hours	0.60 ± 0.02	2.22 ± 0.07
71 hours	0.60 ± 0.02	2.23 ± 0.07
90 hours	0.62 ± 0.02	2.26 ± 0.07
96 hours	0.63 ± 0.02	2.34 ± 0.07
102 hours	0.59 ± 0.02	2.18 ± 0.07
106 hours	0.60 ± 0.02	2.23 ± 0.07
126 hours	0.60 ± 0.02	2.21 ± 0.07
151 hours	0.59 ± 0.02	2.18 ± 0.07

This first test with a sealed mini-TEPC shows that the detector response in keV/µm doesn't change with time, in spite of a fast gas gain reduction in the first hour after the sealing. However, this finding can not be extrapolated to high-LET radiations, as therapeutic carbon-ion beams, since they give rise to about two order of magnitude more ionisation events, which could spoil faster the counting gas.

Chapter 6

Conclusions

Although in this experimental study some measurements with fast neutrons have a relatively poor statistics, bluring the spectral data, some finding has been reached.

The mini-TEPC response to low-LET radiations (gamma rays) does not depend on the ΔV value, apart from the obvious LDT increase with the ΔV decrease, neither on the absolute voltage values at the electrodes.

The mini-TEPC response to high-LET radiations (fast neutrons) is more problematic. A spectral dependence appears due to the absolute voltage values at the electrodes at the same ΔV value:

i)   at high $V_{cathode}$ absolute value, large y-value events are not properly detected, shifting toward lower y-values, hence spoiling the proton-edge;

ii)   at positive V_{anode} values the low-y part of the spectrum is spoiled by a very high electronic noise;

iii)   at negative V_{anode} values the low-y part of the spectrum Is not spoiled and the large y-value events are properly measured, although the $V_{cathode}$ absolute value is high.

More measurements at higher statistics are necessary to confirm the upper-mentioned conclusions. If confirmed, further mini-TEPC versions should be done, with an improved front-end electronics and with a larger electronic-avalanche volume to reduce the charge density occurring with high-LET radiations.

The second aim of the thesis was to test the possibility to use mini-TEPCs in sealed mode, to make them easier to use in the hospital environment. The test, lasted 6 days, has been performed with ^{137}Cs gamma rays. The results are encouraging, showing an almost constant response all over the 6 days. The measured radiation quality, namely $\bar{y}_F$ and $\bar{y}_D$, decreases of about 2% in 6 days. That value is compatible with the lineal-energy calibration uncertainty. If this response stability will be confirmed also for high-LET radiations, sealed mini-TEPCs for clinical use could be constructed.

APPENDIX A

<u>CONSIDERATIONS ON RESTRICTED AND UNRESTRICTED LET</u>

The stopping power S(E) given by the Bethe formula [G. Knoll, 2000] is the conventional quantity to characterize how particles lose their energy along the track when crossing a medium. In 1952, Zirkle introduced a the concept of Linear Energy Transfer (LET) stressing that in dosimetry knowing the energy absorbed by the medium is more relevant than the energy lost along the track. Unfortunately, the collision stopping power in a small volume would overestimate the dose because of secondary electrons escaping from the volume, a possible solution to that problem was to consider the restricted LET which takes into account the energy lost by particle with energy transfers smaller than a certain threshold and is defined as:

$$L_\Delta = \left(\frac{dE}{dl}\right)_\Delta$$

The introduction of the restricted LET offers the opportunity to measure the energy released near the track, which is the one that cause the highest biological effect. High-energy electrons may create secondary ionizations with enough energy to travel far from the point of creation, this phenomenon carries energy away to further regions irrelevant to the local biological effect. The non-restricted LET, LET_∞, includes all energy losses up to the maximum allowed, thus is equal to the negative stopping power.

LET is an average quantity, which cannot be measured in mixed field. Moreover, at the microscopic level we need to consider measurable quantities connected to the stochastic of the energy deposition.

The research to avoid the limitations of the LET concept and study the energy deposition at the microscopic scale using stochastic quantities was initiated by Rossi, Rosenweig and co-workers in 1955 under the name of microdosimetry.

BIBLIOGRAPHY

- R. S. Caswell (1966), *Deposition of energy by neutrons in spherical cavities*, Physics in medicine and biology vol. 16, 611

- S. Chiriotti, D. Moro, P. Colautti, V. Conte and B. Grosswendt (2015), *Equivalence of pure propane and propane TE gases for microdosimetric measurements*, Radiation protection dosimetry vol.1, 1-5

- V. Conte, D. Moro, B. Grosswendt, P. Colautti (2013), *Lineal energy calibration of mini tissue gas-proportional counters (TEPC)*, Multidisciplinary applications of nuclear physics with ion beams (ION BEAMS '12) – AIP conf. proc., v. 1530, 171-178

- L. De Nardo, D. Moro, P. Colautti, V. Conte, G. Tornielli et al. (2004a), *Microdosimetric assessment of Nice therapeutic proton beam biological quality*, Physica Medica vol. XX, 71-77

- L. De Nardo, V. Cesari, N. Iborra, V. Conte, P. Colautti et al. (2004b), *Microdosimetric investigation at the therapeutic proton beam facility of CATANA*, Radiation Protection Dosimetry vol. 110, 681-686

- L. De Nardo, P. Colautti, J, Hérault, V. Conte, D. Moro (2010), *Microdosimetric characterisation of a therapeutic proton beam used for conjunctival melanoma treatments*, Radiation Measurements vol. 45, 1387-1390

- M. Durante and J. S. Loeffler (2010), *Charged particles in radiation oncology*, Nature reviews clinical oncology vol. 7, 37-43

- U. Fano (1954), *Note on the Bragg-Gray principle for measuring energy dissipation*, Radiation research vol. 1, 237-240

- K. Gunzert-Marx, H. Iwase, D- Schardt, R. S. Simon (2008), *Secondary beam fragments produced by 200 MeV/u 12C ions in water and their dose contributions in carbon ion radiotherapy,* New Journal of Physics vol. 10(7):075003

- IARC (2014), Agency for Research on Cancer, *World cancer report 2014*.

- ICRU 36 (1983), *Microdosimetry*, International Commission on Radiation Units and Measurements, *ICRU report 36*

- ICRU 49 (1993), *Stopping powers and ranges for protons and alpha particles,* International Commission on Radiation Units and Measurements

- ICRU 85a (2011), *Fundamentals quantities and units for ionizing radiations (revised)*, International Commission on Radiation Units and Measurements

- O. Jäckel (2010), *Radiotherapy with protons and ions beams*, La Rábida 2009, International scientific meeting on nuclear physics : Theory, Experiments and Applications

- O. J. Kelada (2011), *The potential advantages and disadvantages of cancer therapy using charged particles compared with megavoltage x-rays*, PTCRI, Particle Therapy Cancer Research Institute, official website

- G. F. Knoll (2000), *Radiation Detection and Measurements*, Wiley and sons, third edition

- T. Loncoln, V. Cosgrove, J. M- Denis, J. Gaulette, A. Mazal et al. (1994), *Radiobiological effectiveness of radiation beams with broad LET spectra: Microdosimetric analysis using biological weightening functions,* Radiation Protection Dosimetry vol. 52, 347-352

- N. Matsufuji (2007), *Specification of carbon ion dose at the national institute of radiological sciences (NIRS),* Radiation research vol. 48, A81-A86

- K. Mitev, P. Segur, A. Alkaa, M. Bordage, C. Furstoss et al. (2005), *Study of non-equilibrium electron avalanches, application to proportional counters*, Nuclear Instruments and Methods in Physics research Section A: Accelerators, Spectrometers, Detectors and Associated Equipment, vol. 13, 396-400

- D. Moro (2006), *Development of tissue equivalent proportional counter for BNCT microdosimetry*, PhD thesis, Università degli studi di Ferrara

- E. Motisi (2015), *Development of microdosimetric techniques applied to hadron therapy*, Master thesis, Universtà degli Studi di Padova

- H. Paganetti (2003), *Significance and implementation of RBE variations in proton beam therapy*, Technology in cancer research & treatment vol. 2, 413-426

- P. Pihet, H. G. Mendel, R. Schmidt, M. Baudin and A. Wambersie (1990), *Biological weighting function RBE specification of neutron therapy beams.* Intercomparison of 9 European centres, Radiation Protection Dosimetry

- PTCOG (2017), Particle therapy co-operative group, *Patient statistics* (updated 9 Nov. 2014)

- P. Segur, P. Olko and P. Colautti (1995), *Numerical modelling of tissue – equivalent counters*, Radiation Protection Dosimetry vol. 61, 323-350

- M. Scholz, A. M. Kellerer, W. Kraft-Weyrather, G. Kraft (1997), *Computation of cell survival in heavy ion beams for therapy. The model and its approximation,* Radiation and Environmental Biophysics vol. 23, 249-252

- S. Tegami, S. D. Bello, S. Luan, A. Mairani, K. Parodi, M. H. Holzscheiter (2017), *LET Monitoring Using Liquid Ionization Chambers,* International Journal of Medical Physics, Clinical Engineering and Radiation Oncology, Vol. 06 No. 02

- W. Tinganelli, N. Y. Ma, C. Von Neubeck, A. Maier, C. Schicker et al. (2013), *Influence of acute hypoxia and radiation quality on cell survival*, Journal of Radiation Research vol. 54, 23-30

- K. Weyrather and G. Kraft (2004), *RBE of carbon ions: experimental data and the strategy of RBE calculation for treatment planning*, Radiotherapy and Oncology vol. 73, S161-S169

ACKNOWLEDGMENTS

This journey into microdosimetry has come to an end, fortunately it is not a definitive farewell, in few weeks it will start again.

These months were instructive and helped me to grow both as a person and as a physicist. For this reason, I want to thank all the people that supported me during this experience.

First of all I want to thank my thesis supervisor, Dr. Marco Mazzocco, for giving me the opportunity to start this journey.

I want also to express my gratitude to the group in Legnaro for the warm welcome in Legnaro National Laboratories and all the support they gave me in these months.

I want to thank Dr. Valeria Conte for introducing me to the world of microdosimetry, for helping me when I felt discouraged finding always a solution to make me feel better.

I want also to thank Dr. Paolo Colautti who shared his huge experience in this field with me giving me the opportunity to learn what experimental microdosimetry means. Obviously, I cannot forget to thank Dr. Anna Selva who supported, guided and helped me in measurements and analysis even if the deadline of her PhD thesis was forthcoming too.

The last, but obviously not the least, that I want to thank is my big extended family. They have always encouraged me even in bad moments when I wanted to give up; they stayed besides me patiently giving me their precious advices. Thanks to them, I have understood that I have found my way and that I must be grateful for that because it is not so easy to achieve this goal nowadays.

I want also to thank everyone stayed besides me in these years, they are too much to write them all but they now that I am thankful.